



MINISTERUL
EDUCAȚIEI ȘI
CERCETĂRII
ȘTIINȚIFICE

OIPOSDRU



Universitatea POLITEHNICA
din București

University POLITEHNICA of Bucharest
Doctoral School of Industrial Engineering and Robotics

University of Pitesti
Interdisciplinary Doctoral School

Ing. BOȘNEAG F. Ana (GOGORICI)

PhD THESIS

Summary

**Contributions to the study and development on friction stir
welding process and system with rotating active element of
different aluminium alloy structures**

Scientific Supervisors,

Prof. univ. dr. ing. Marian GHEORGHE

Prof. univ. dr. ing. Eduard Laurențiu NIȚU

- 2020 -

Table of contents

	R	T
Keywords	2	-
<i>Foreword</i>	3	5
Introduction	4	6
Legend	-	7
<i>Part I. Current state of research – development and industrial applications of friction stir welding with rotating active element</i>		
<i>Chapter 1. Welding procedures by friction stir welding</i>	5	9
1.1. Introduction regarding the friction stir welding process	5	9
1.2. Advantages and limitations of the friction stir welding process	-	10
1.3. Working principle and process parameters of the FSW process	5	11
1.4. Types of FSW welding process	6	13
1.5. Types of welded materials using the FSW process	6	14
1.6. Active welding elements for FSW	7	18
1.7. FSW welding equipment	7	20
1.8. FSW industrial applications	8	21
<i>Chapter 2. Characteristics of friction stir welding joints</i>	9	25
2.1. Categories of characteristics of welded joints and evaluation procedures	9	25
2.2. Macrostructure and microstructure of welded joints	9	25
2.3. Defects of welded joints and the connection between their appearance and the process parameters	10	33
2.4. Mechanical properties of welded joints	11	35
<i>Chapter 3. Researches on modeling and numerical simulation of the friction stir welding process.</i>	12	39
3.1. General stages of numerical modeling and simulation	12	39
3.2. Defining the geometry of the part and the rotating active element	-	42
3.3. Defining the behavior of materials (constituent equation)	-	42
3.4. Modeling of heat transfer	-	43
3.5. Definition of contact between surfaces	-	44
3.6. Setting the boundary conditions	-	45
3.7. Mesh of the numerical model	-	46
3.8. Methods for validating the numerical models of the FSW process	14	48
3.9. Results of the simulation of the FSW process of structures of different materials	15	52
<i>Chapter 4. Conclusions on the current state of research – development and industrial applications of friction stir welding with rotating active element</i>	16	55
<i>Part II. Contributions to the theoretical – experimental research and numerical modeling on the process and system of friction stir welding with rotating active element of different aluminium alloy structures</i>		
<i>Chapter 5. The directions, the main objective and the research - development methodology regarding the friction stir welding of different aluminum alloy structures</i>	21	59
5.1. Research and development directions	21	59
5.2. The main objective of the research - development activity	21	59
5.3. Research - development methodology	-	59
<i>Chapter 6. Elements of the experimental research system for the friction stir welding of different aluminum alloy structures</i>	23	67
6.1. Characteristics of the component plates of the welding structure materials	-	67
6.2. The experimental stand and the process characteristics measured in real time	23	68
6.3. Welding rotating active element	24	71

6.4. Defining and production of welding parts	24	71
6.5. Defining and sampling of the sample for characterisation of joint made	24	73
6.6. Coding of experiments and specimen	-	75
6.7. Preparation of specimens	25	76
6.8. Measuring the roughness of the welding seam	26	78
6.9. Macroscopic and microscopic analysis	26	79
6.10. Measurement of microhardness	26	79
6.11. Measurement of tensile strength	26	81
<i>Chapter 7. Results of the preliminary theoretical - experimental research on the friction stir welding process and system of different aluminum alloys structures</i>	<i>27</i>	<i>83</i>
7.1. Process temperature	27	83
7.2. Axial process force	28	86
7.3. The roughness of the welding seam	29	91
7.4. The macrostructure of welding seam	30	93
7.5. The microstructure of the welding seam	32	104
7.6. The microhardness of the welding seam	33	109
<i>Chapter 8. Results of the advanced theoretical - experimental research on the friction stir welding process and system of different aluminum alloys structures</i>	<i>35</i>	<i>119</i>
8.1. Advanced experimental program	35	119
8.2. Process temperature and axial process force	35	119
8.3. The roughness of the welding seam	37	123
8.4. The macrostructure of welding seam	37	124
8.5. The microstructure of the welding seam	38	129
8.6. The microhardness of the welding seam	39	130
8.7. The tensile strength of the welded structure	40	134
8.8. Case study on analysis of structures by tensile strength test and digital image correlation	43	142
<i>Chapter 9. Numerical modeling of the friction stir welding process of different aluminum alloy structures</i>	<i>44</i>	<i>147</i>
9.1. Building the numerical model	44	147
9.2. Validation of the numerical model	45	151
<i>Chapter 10. Final conclusions and main contributions to the development and numerical modeling of the process and system of friction stir welding with rotating active element of different aluminum alloy structures</i>	<i>47</i>	<i>157</i>
Selective references	51	161

Keywords

friction stir welding,
aluminum alloys,
process temperature,
axial process force,
roughness,
macrostructure,
microstructure,
microhardness,
tensile strength,
digital image correlation,
numerical modeling.

Foreword

Theoretical - experimental research and numerical modeling of the friction stir welding process of different aluminum alloy structures, AA2024, AA6061 and AA7075, used in the aeronautical industry, in order to determine the conditions that will lead to the construction of welded structures with superior properties, represents the *motivation* and *direction* of the doctoral studies, finalized by the present doctoral thesis.

The doctoral program consisted of the preparation, presentation and support of the examinations and the scientific reports, the study depth, the proposal and the development of a research methodology, theoretical and experimental research to determine the influence of the process parameters and of the structure characteristics on the quality of the joints welded by friction stir welding, developing a specific numerical model, carrying out and publishing scientific papers, as well as developing the present doctoral thesis on the contributions to the study and development of welding processes and systems by friction stir welding of different aluminum alloy structures.

I express profound thanks to Mr. Prof.univ.dr.ing. Marian GHEORGHE and Mr. Prof.univ.dr.ing. Eduard Laurențiu NIȚU, for the scientific guidance and coordination of the entire activity of completing the doctoral program, the support, full confidence and total availability granted during this period.

I express my sincere thanks to Mr. ing. Radu COJOCARU and Mr. ing. Cristi CIUCĂ from the "National Institute for Research - Development in Welding and Material Testing" - ISIM Timisoara, for the support given to the welded joints.

I express my thanks to Mr. Conf.univ.dr.ing. Claudiu BĂDULESCU from ENSTA Bretagne, under whose guidance Mr. ing. Ovidiu CRĂCĂNEL, Mr. Conf.univ.dr.ing. Jan GRIGORE and Ph.D. Denis NEGREA contributed to the determination of some mechanical properties of the joint.

I wish to express my sincere thanks to Mrs. Conf.univ.dr.ing. Daniela Monica IORDACHE for the support and availability granted during this period for the realization and validation of the numerical model.

I express my sincere thanks to Mr. Prof.univ.dr.ing. Tom SAVU and Mr. Prof.univ.dr.ing. Nicolae IONESCU - from the POLITEHNICA University of Bucharest, Mr. Conf.univ.dr.ing. Alin Daniel RIZEA - from the University of Pitești, Dr. Eng. CSP 1 Diana Mura BADEA - from the National Research Institute for Mechatronics and Measurement Technique - Bucharest, for comments and recommendations addressed to the Commission for the evaluation and public support of the doctoral thesis.

I am grateful to my family, to the current colleagues of the company where I carry out my activity and to my PhD colleague, ing. Adrian Marius CONSTANTIN, for the moral support and the understanding manifested during all the doctoral studies.

The activities within the doctoral studies were carried out at the POLITEHNICA University of Bucharest and the University of Pitești, according to the Doctoral Collaboration Agreement concluded between the two institutions. Also, part of the activities regarding the elaboration of this doctoral thesis benefited from the support of the Sectoral Operational Program for Human Resources Development (POS DRU), financed by the European Social Fund and the Government of Romania, by contract no. POS DRU / 187 / 1.5 / S / 155536.

Boșneag F. Ana (Gogorici)

Introduction

In the current tendency context of replacing or improving the classical procedures, minimizing costs and using materials with superior properties, an important role is to extend the research to the area of joining different materials using the friction stir welding process (FSW).

The research and development activity within the doctoral preparation is an integral part of the author's scientific concerns in the field of friction stir welding process for joining three different aluminum alloys.

* * *

In the first part of the doctoral thesis, in relation to the current state of research - development, is presented relevant data on friction welding processes and systems with rotating active element - generalities of the welding process by friction stir welding, advantages, limitations, joined materials, active welding elements, welding equipment, industrial applications, categories of characteristics of welded structures and evaluation processes, macrostructure, microstructure and defects, microhardness, strength and ductility of welded joints, numerical modeling and simulation of the FSW process, conclusions.

In the second part of the doctoral thesis, considering the data and conclusions drawn from the analysis of the current stage, as well as the research and development directions regarding the processes and systems of friction stir welding, it is determined that the main research and development objective in the doctorate: the process and system development of friction stir welding with rotating active element of different aluminum alloy structures, through theoretical - experimental research and numerical modeling.

In the next, the research - development methodology is conceived as a reference system for the actions to achieve the main objective of the doctoral activity and for future developments. Theoretical researches - preliminary and advanced experimental, complex and high volume, have led to the achievement of four different types of welded structure under different welding technological conditions, with the measurement of temperature and axial process strength, sampling, analysis of some characteristics of the welding seam and the surrounding areas - roughness, macrostructure, microstructure, micro-hardness and tensile strength, graphical representation of specific dependency relationships, highlighting representative correlations and conclusions. Also, a valid numerical model was developed for simulating the FSW joint of three different aluminum alloys.

In the last part of the doctoral thesis, the general conclusions and main contributions of the doctoral thesis are presented in order to achieve the main objective of the doctoral research – development activity, the scientific importance of the doctoral thesis, the practical importance of the doctoral thesis, as well as perspectives of development of FSW processes for determining optimum welding conditions and characteristics of welded joints for various materials, geometries, production volumes etc.

Part I.

Current state of research – development and industrial applications of friction stir welding with rotating active element

Chapter 1. Welding procedures by friction stir welding

1.1. Introduction regarding the friction stir welding process

Friction stir welding, FSW, is a solid-state welding process, invented by Thomas and his collaborators, in 1991 at The Welding Institute "TWI" in Cambridge, UK (FSW: Friction Stir Welding) [T06]. Before being made popular by TWI, the principle of solid state welding was first certified in 1956 in the Soviet Union. This technology was initially used for welding aluminum alloys in classes classified as non-weldable alloys by using classical welding techniques [M12]. This process is considered to be one of the most significant welding achievements of the last period [K06].

1.3. Working principle and process parameters of the FSW process

In the welded joint area, the materials can have either a plastic or a melted state, so that there is a continuity in the material structure of the joined parts. The welding process in solid state is considered to be the oldest welding process, being used since the discovery of the iron, by welding to the forge fire and hammering the iron bars heated to red. Among the processes of welding by pressure in solid state and without melting of the basic material include friction stir welding with rotating active element (Friction Stir Welding – FSW), this being a welding variant without melting the basic material developed from a dynamic point of view. [M04].

Standard welding procedures are not suitable for welding different materials [K06].

The working principle of the FSW can be defined as follows: a cylindrical active element, with a rotational movement and a translational one penetrates the material, in the area of the welding joint, moves along it and exits the material at the end of the welding seam (Fig. 1.3.1). When the shoulder of the active element reaches the surface of the welding materials a significant amount of heat generated by the friction is released in the contact area. The increase of the temperature plasticises the material, still remaining in solid state, at approx. 70 – 90% of the melting temperature. The combined effect of the temperature generated and the pressure exerted by the active element allows the material to be mechanically mixed [K09].

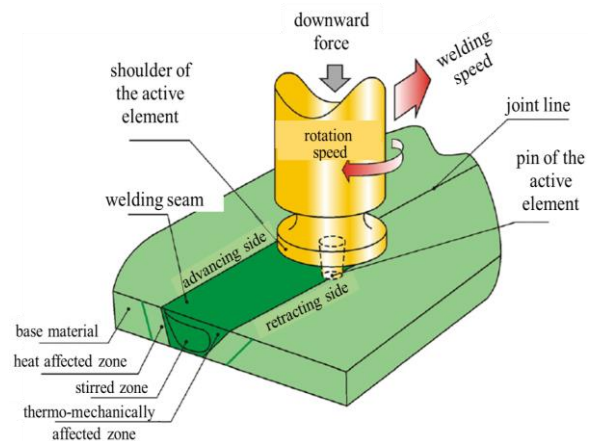


Fig. 1.3.1. The working principle of FSW procedure [K02]

The quality of the welding seam made depends, first of all, on the process parameters set for the process execution. The process parameters for FSW are: the rotation speed of the active working element [rpm], which directly influences the temperature increase in the welding seam area, the welding speed [mm/min] and the inclination angle of the active element [M09]. The inclination angle of the active element has the role of pushing the material to be processed under its shoulder, to lead to the gradual forging effect, realized in the material, during the process. At the same time, the inclination angle of the active element prevents the material from flowing sideways, thus ensuring that the weld is closed on the back of the pin [B02].

The welding speed of the active element is one of the most important input parameters of the process, because it generates and controls the degree of mixing and homogenization of the welding materials, moving the material in front of the pin behind it. A high rotation speed value generates an increase in temperature due to the higher frictional force and mixing of the base materials [C03].

Another important feature of the FSW process is the depth of penetration of the pin of the active element in the welding materials, which is directly responsible for the quality of the welding. When the penetration depth is less than optimal, the shoulder of the active element does not come in contact with the surface of the workable materials or, if the value is greater than the optimal one, a very prominent trace of the shoulder is created along the welding seam [C03]. When determining the penetration depth, the length of the active element's pin is taken into account, and this must be chosen in accordance with the thickness of the joints: the length of the pin is smaller than the thickness of the base plates, and its diameter is slightly larger than the thickness of the base plates [P05].

1.4. Types of FSW welding process

Examples of technologies that use friction stir welding process can be considered the following:

- friction stir welding, spot friction stir welding or hybrid friction stir welding with rotating active element (Fig. 1.4.1);
- friction processing with an active rotating element;
- friction channels with active rotating element;
- stamping and deformation by friction with an active rotating element;
- making unconventional shapes using the friction process with rotating active element;
- microforming by friction with rotating active element [A08].

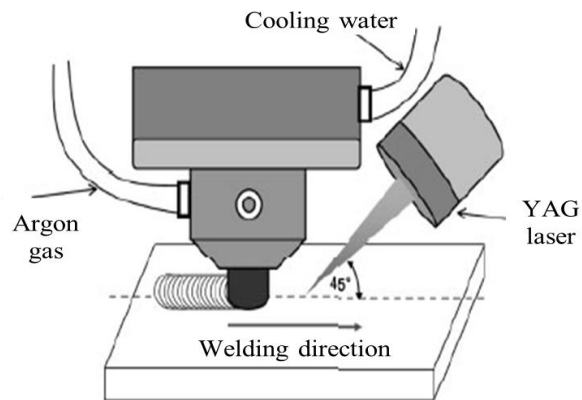


Fig. 1.4.1. Hybrid FSW [S12]

An important branch of the friction stir welding process is the hybrid friction stir welding process (HFSW), developed for joining high melting point materials [C01]. This process is a combination between FSW and another traditional welding process, with FSW playing the dominant process role, and with the second process playing a secondary role, in order to preheat the parts [C01]. So far, FSW has been combined with: YAG laser, TIG arc [C13, C14, C15] and plasma arc, but the most common hybrid pair is: FSW combined with laser, generically called friction stir welding process with assisted by laser (LAFSW) (Fig. 1.4.1) [B08].

1.5. Types of welded materials using the FSW process

The friction stir welding processes, FSW, were initially developed to weld plates from aluminum alloys, this being a less hard and slightly malleable material [B05]. Over time, due to the efficiency of the process, the studies have expanded to the combination of materials such as: polymeric materials [K10], metal materials - brass, copper [C12, C13, C14], magnesium, titanium, steel [L02] and composite materials with metal matrix of aluminum, copper and titanium, and ceramic reinforcement of particles such as Al_2O_3 (aluminum oxides), SiC (silicon carbide), Si_3N_4 (silicon nitrides) and B_4C (boron carbide) [B09, M06]. The polymeric materials welded by this process are the polypropylene materials [K10] and composite materials with polymeric matrix of polypropylene reinforced with 30 % fiberglass [C18].

Using the FSW process, can be welded, similar materials, of the same types or different types, from different materials, with different properties. In the case of different metals, conventional welding is difficult to achieve due to the large differences in physical properties, such as thermal conductivity, melting point, thermal expansion, which leads to high distortions, residual stresses and irregularities in metallurgical characteristics of the welding seam, resulting in broken joints [B03, M07]. The friction stir welding process (FSW) proves to be the optimal alternative, as it eliminates the melting points of the two different materials. This additional function of the FSW represents a superior net advantage over other joining processes.

1.6. Active welding elements for FSW

The active welding element used in FSW joints plays three main roles:

- to heat the work pieces;
- to agitate, mix and move the plasticized material after heating;
- to control and restrict the movement of the material in its shoulder area [A08].

Regarding the shape, the FSW active welding element has two important parts: the shoulder, which comes into contact with the welding material, and the pin, which penetrates the welding material.

The shoulder of the active element has the role of producing heat on the surface of the welding areas and in their immediate vicinity, by rubbing with the welding materials. Thus, the diameter of the shoulder is one of the extremely important characteristics when defining the geometry of the active element. A larger diameter increases the pressing force and implicitly the temperature during the process, having a positive influence on the mechanical properties of the joint [P10, S17]. Another important feature is the reference form of the main shoulder surface, which can be: concave (standard shoulder shape), convex and flat.

The pin of the active element causes deformation of the material and heats it up inside the welding seam by moving the material in front of the active element behind it. Like the shoulder of the active element, its pin can have different forms, respectively: smooth cylindrical, threaded cylindrical, grooved cylindrical, flattened cylindrical, smooth conical, threaded conical, with convex tip and other combinations.

The material of the active element is very important, because the active element works under difficult conditions. The expected characteristics of its material are: resistance and stability at high temperatures, wear resistance, resistance to breakage, high coefficient of thermal expansion and workability [A08]. The material of the active element is chosen according to the characteristics of the material/ materials to be joined [M04]. When choosing the active element for welding different materials, the properties of the material with the highest thermal coefficient are taken into account.

1.7. FSW welding equipment

FSW welding can be performed on milling machine or FSW welding machine. FSW welding machines have the advantages of handling, positioning, gripping the blanks and controlling the process during its construction.

A new direction for technology in this area is robot welding. This has many advantages, such as flexibility in making complex welds from different/ composite directions. A disadvantage of the robotic welding is the low stability in relation to the action of high value processing forces.

1.8. FSW industrial applications

Indicators of FSW development in industrial applications

The friction stir welding process, FSW, is currently the process with one of the fastest ascents. Despite the fact that this process appeared more than 29 years ago, it is in continuous development and the area of use increases from year to year. FSW licenses and patents were directed to the following development sectors: more than 50 % to the transport area (auto, rail, aeronautical, aerospace and naval), and the rest to other areas such as metal processing, research and development, electronics, development of machines and equipment etc. [M01].

Applications of FSW welding in the aeronautical industry

Finding the applicability of this welding process, FSW, in the aeronautical industry for the joining of aluminum alloys of aircraft is easily intuitive due to the fact that the fuselage of an aircraft is built from 20 - 50 % of aluminum alloy [T02]. Also, the applicability of the FSW process in the aeronautical industry has been under investigation for more than 30 years. The most common aluminum alloys used in the aviation industry are AA6061, AA2024 and sometimes AA7075. Currently, there is also applicability for large welding seam lengths, examples including large fuel tanks and other spacecraft vehicle containers.

The first company to decide to replace the rivet with FSW, when making the Eclipse 500 aircraft (Fig. 1.8.5) is Eclipse Aviation Corporation. Using the FSW welding of the fuselage and wings of the Eclipse 500, the following advantages were obtained: the number of rivets used decreased by 60 - 70 % [J02], saving time due to the process in one step (instead of drilling and the weight of the final product was significantly reduced, and the risks assigned to the classic assembly procedures were eliminated [M12]



Fig. 1.8.5. Applications of FSW welding in the aeronautical industry [J02]

Applications of FSW welding in the automotive industry

The automotive industry aims to reduce the weight and increase the resistance of standard vehicles, which can be achieved by using alloys from different aluminum series and the friction stir welding process, FSW.

The friction stir welding process is used in the automotive industry, in the mass production by Mazda Motor, in the making of the hood and the luggage compartment door of the Mazda RX-8, as well as in the rear doors of the Mazda MX-5, when making the suspensions and assembling the door handles for some Ford models [J02].

Other industrial applications of FSW welding

In the last decade, the FSW welding process has been explored by several industries, such as aerospace, automotive, maritime, armament, nuclear etc. The first company that used this process in the mass industry was the Norwegian company "Marine Aluminum" [J02]. FSW welding has already been successfully applied to joints within tanks, maritime structures, train panels, air frames and vehicles [K06].

Chapter 2. Characteristics of friction stir welding joints

2.1. Categories of characteristics of welded joints and evaluation procedures

The quality indicators of the welded joints through the FSW process can be considered as follows: the microstructure of the welded joints, the precipitation state in the welding seam, the texture of the welded joints, the remaining tensions, the lack of defects inside the welding seam, the micro-hardness and the tensile strength etc. for welding seam, areas adjacent to the welding seam, welded structure.

2.2. Macrostructure and microstructure of welded joints

Macrostructure of welded joints

Macrostructural, the welding seam and its adjacent areas are: WZ, TMAZ, HAZ, and BM [B16] as follows (Fig. 2.2.1).

1. WZ (weld zone) is the welding zone, which is affected both thermally and mechanically by the pin and shoulder of the rotating active element.

2. TMAZ (thermo mechanically affected zone) is the area that is thermally and mechanically affected, which is close to the core of the welding seam and in which the material is plastic deformed and thermally affected by the heat released during the process.

3. HAZ (heat affected zone) is the heat affected area, which is close enough to the welding seam so that the thermal cycle from the moment of the process changes its microstructure, but does not deform it plastic.

4. BM (base material) is the base material, respectively, the part of the material that is not thermally and mechanically affected.

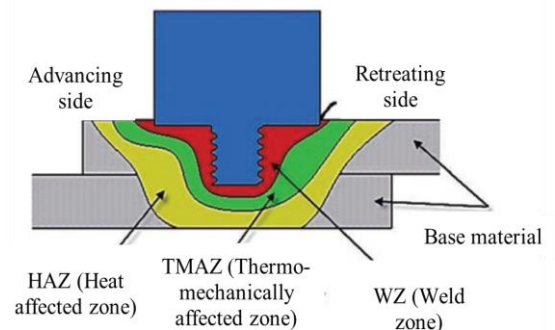


Fig. 2.2.1. Macrostructural areas of the FSW welding seam [B16]

The macrostructural analysis highlights the defects in the welding seam, the thermally influenced areas, the base metal and the shape of the welding area. In the FSW process, the shape of the welding seam section and the distribution of the four characteristic areas are very important, being able to give information on the efficiency of the working regime, the correctness of the chosen active element and the properties of the joint.

Microstructure of welded joints

The analysis of the evolution of the microstructure of the FSW joints can be complicated because in the welding seam area there is a plastic deformation and a dynamic recrystallization of the materials used. Analyzing the microstructure of the FSW joint from the point of view of the four macrostructural areas, we found a refining of the grains as the distance decreased from the core of the welding seam.

Aluminum alloys AA6061 (retraction part) and AA2024 (advance part) were welded FSW using a threaded cylindrical pin. From the microstructural point of view in the area of the two basic materials, no significant changes were identified, although the process used involves a considerable amount of energy and heat released during the process. The heat affected zone (HAZ) is considerably influenced by the thermal cycle related to this process, the differences between it and the basic material are major (Fig. 2.2.8: b and f). The thermally and mechanically affected zone (TMAZ) shows a considerable increase in the grain boundaries due to the plastic deformation during the process and less to the thermal factor (Fig. 2.2.8: c and e). In the weld zone (WZ), the basic materials underwent a major plastic deformation, which resulted in fine echial grains (Fig. 2.2.8: d). The shape and dimensions of the core kernels lead to a considerable improvement of the mechanical strength of the welding seam [S01].

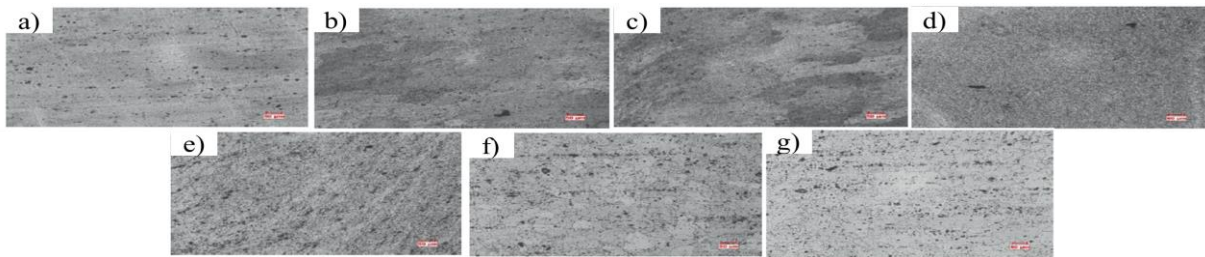


Fig. 2.2.8. Microstructure of the various areas of the FSW seam between AA6061 and AA2024:
a) base material AA2024; b) HAZ for AA2024; c) TMAZ for AA2024; d) WZ;
e) TMAZ for AA6061; f) HAZ for AA6061; g) base material AA6061 [S01]

Texture of welded joints

From the point of view of the visual aspect of the FSW welding seam on the upper surface, the one that comes into contact with the shoulder of the active element, there are semicircular traces, in the form of "onion sheets" (Fig. 2.2.15). The surface opposite the area of direct contact with the active element does not show any obvious changes after the welding seam is made.

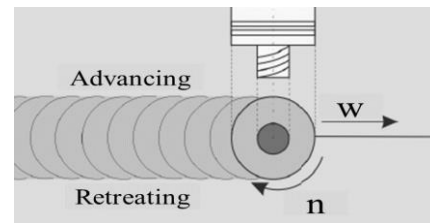


Fig. 2.2.15. The visual aspect of the welding seam FSW [M15]

Remaining stresses in welded joints

Based on the weld seam geometry, the highest residual stresses appear longitudinally, parallel to the welding direction, in the TMAZ area, on the feed side of the active element [C09, R03]. The transverse residual stress has no dependence on the welding process [C01].

It has been found that the residual stresses present in FSW welded joints usually have an "M" shape distribution and that the longitudinal stresses are greater than the transverse stresses. Although this distribution is almost symmetrical, the residual stress are usually slightly higher on the advancing side of the active element [B16, C09] (Fig. 2.2.19).

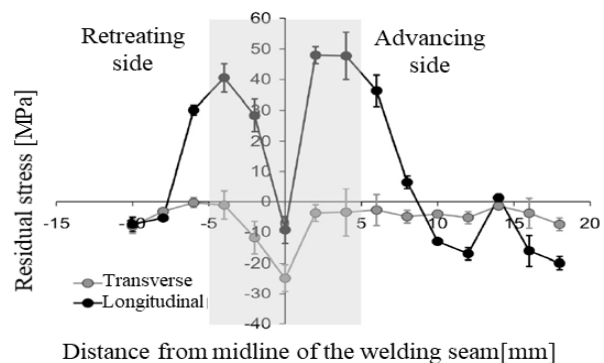


Fig. 2.2.19. Residual stress distribution in FSW welding seam [C09]

2.3. Defects of welded joints and the connection between their appearance and the process parameters

The FSW process is predisposed to the appearance of defects, different from the defects registered in the classical welding procedures. The input parameters of the FSW, such as: rotation speed, welding speed, characteristics of the active element (shape and dimensions), can lead to the occurrence of defects if not set properly. In particular, the welding pin plays a very important role in achieving the quality of the welding seam. An equally important role is played by the depth of penetration of the active element during the process [K06, N01]. The combination of these characteristics can lead to the production of excessive heat, insufficient heat, insufficient or excessive mixing and insufficient shoulder pressure on the realized welding seam.

The defects encountered in performing the FSW process may be visible: jagged seam or scales (Fig. 2.3.1), excessive burrs (Fig. 2.3.2), crack along the welding seam, intermittent or continuous (Fig. 2.3.3) or uneven seam (Fig. 2.3.4) [B01].

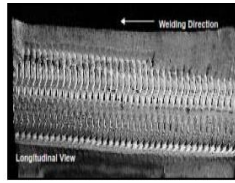


Fig. 2.3.1. Scales / rattan seam [B01]



Fig. 2.3.2. Excessive burrs [B01]

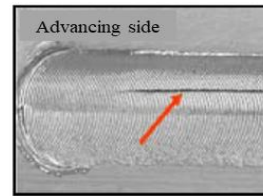


Fig. 2.3.3. Crack along welding seam [B01]



Fig. 2.3.4. Uneven seam [B01]

The second category of defects is represented by the defects in the macrostructure of the welding seam. These defects cannot be identified with the naked eye, and macroscopic analysis is required for their attestation. As with surface defects, they can be of various forms: tunnel or "wormhole" defects (the most common macrostructural defects) (Fig. 2.3.5), collapsed core defects (Fig. 2.3.9), defect due to the lack of penetration (Fig. 2.3.10) and defect of the "kissing bond" type (Fig. 2.3.11).



Fig. 2.3.5. Worm tunnel or hole [B01]

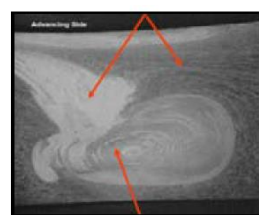


Fig. 2.3.9. Crushed core [B01]

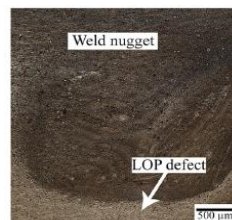


Fig. 2.3.10. No penetration [K05]

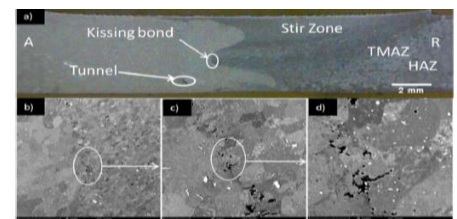


Fig. 2.3.11. *Kissing bond* defect [K06]

In conclusion, it can be said that the prevention of defects can be achieved by improving the heat input introduced into the welding area and controlling it during the process.

2.4. Mechanical properties of welded joints

Microhardness of welded joints

From the analysis of the distribution of microhardness of three welding seams made with different active elements, major differences were identified between the results made with a smooth cylindrical pin and with a threaded cylindrical pin, respectively, the microdurities are higher in the cord made with the threaded pin [K12].

The microhardness of the welding seam made between AA7003 and AA6060, with a threaded cylindrical pin, the rotation speed of 1000 rpm and the welding speed of 40 mm/min, is measured in the cross section, in the middle of the welding seam (Fig. 2.4.3). The asymmetrical distribution of the microhardness of the welding seam is due to the very different values of the microhardnesses of the two basic materials.

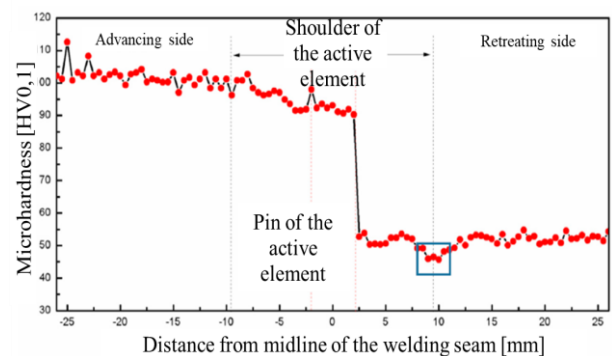


Fig. 2.4.3. Microhardness of FSW joints for AA7003 and AA6060 [D10]

The microhardness of the welding seam is influenced by both the process parameters and the pin shape of the active element used. For the experiments in which two different aluminum alloys are welded, with large differences of the microdurities of the basic materials, the microhardness of the welding seam can be negatively influenced by the material with the lowest microhardness. In WZ and TMAZ where the materials are mechanically mixed it is clear that the value of the microhardness will be lower than the microhardness of one of the base materials.

Resistance and ductility of welded joints

The tensile strength of FSW welded samples represents approximately 68 – 73 % of the strength of the basic materials. It has been shown that the tensile strength has a tendency to decrease after FSW joining, compared to the base material [K12].

A significant influence on the properties of the joint, implicitly on the tensile strength in welded joints, has the geometry of the active element. As with the values of microhardness, it was shown that the best results were obtained for the joints made with threaded cylindrical pin [K12].

Using the parameter optimization method, Taguchi L16, for the characterization of the FSW joint of two different aluminum alloys, AA5454 and AA7075, was followed to optimize the input parameters to improve the mechanical properties of the welding seam (tensile strength and ductility). The optimum parameters and the process conditions determined for obtaining the highest welding value of the STU are: rotation speed of 1225 rpm, welding speed equal to 21 mm/min, conical profile of the pin, AA5454 on the feed side, inclination angle of the of the rotating active element by 2° and the penetration depth of 0,1 mm. The maximum efficiency of the joint obtained, compared to the resistance of the softer metal used to make the welding seam, is 85.3 %.

In order to obtain the highest values of ductility, the optimal parameters determined are: rotation speed of 1225 rpm, welding speed equal to 21 mm/min, cylindrical profile of the pin, AA5454 on the feed side, the inclination angle of the rotating active element of 1,5° and the penetration depth equal to 0,1 mm [E01].

Chapter 3. Researches on modeling and numerical simulation of the friction stir welding process

3.1. General stages of numerical modeling and simulation

Modeling and simulating the FSW process is a great challenge for any researcher due to the complexity of the process and the large deformations that occur during the joint. One of the advantages of the simulation is that results can be obtained regarding the effect of the process parameters on the quality of the weld, without physically realizing the joint and without consuming material resources and energy [P07]. With the numerical simulation of the welding process FSW can be visualized and analyzed the material flow, temperature range, stresses, deformations and defects, and these can be obtained more easily than by experimental methods [D07].

In order to create an instrument that allows to evaluate the structural behavior of a joint, it is necessary to define a detailed and fully parameterized numerical model, using the finite element method. A high level of finite element model accuracy is also required and is often used for evaluation by comparison with experimental data [F01]. When the numerical model is realised, several elements must be taken into account, such as: the geometry of the parts and the active element, the behavior of the material during the process, the type of contact between the friction surfaces and the friction law, the limit conditions and process parameters, the discretion of the welding parts and instruments. In modeling the process it is essential to keep the model objectives and, at the same time, it is important to adopt an appropriate level of complexity. In this sense, both analytical and numerical methods have a role to play [M09].

When performing numerical modeling, two types of process modeling techniques can be adopted: fluid dynamics (simulation of material flow and temperature distribution) and solid mechanics (simulation of temperature distribution, stresses, and deformation) [D07]. For performing the numerical model for the friction stir welding process, it is necessary to follow the following steps [C10]:

1. Defining the part geometry and the active welding element;
2. Defining the behavior of the material (elasto-plastic or elasto-viscoplastic) by a law of behavior;
3. Definition of elastic properties and heat transfer;
4. Defining the type of contact between surfaces and the friction law;
5. Establishing boundary conditions and process parameters;
6. Discretion of the active work item and parts.

An extremely important feature that must be taken into account when making the numerical model is the geometry of the active element and the welding parts. When designing 2D or 3D models, including FSW process modeling, the shape, dimensions and location in the work system must be taken into account, both for the parts to be welded and for the rotating active element. It is necessary that they correspond to reality in order to obtain a most relevant result.

Besides the dimensional aspect, another important feature of modeling is the law of behavior of materials. In most studies, the constitutive mathematical model used to define the material in numerical simulation is Johnson-Cook, generally the behavior of the materials is viscous-plastic (rel. 3.1.1 and rel. 3.1.2) [J03].

where:

$$\bar{\sigma} = [A + B \cdot (\bar{\epsilon}^{pl})^n] \left[1 + C \cdot \ln \left(\frac{\dot{\bar{\epsilon}}_{pl}}{\dot{\epsilon}_0} \right) \right] (1 - \hat{T}^m) \text{ [GPa]} \quad (3.1.1)$$

$$\hat{T} = \begin{cases} 0, & \text{pentru } T < T_{ref} \\ \frac{T - T_{ref}}{T_{solid} - T_{ref}}, & \text{pentru } T_{ref} \leq T \leq T_{solid} \\ 1, & \text{pentru } T > T_{solid} \end{cases} \text{ [}^\circ\text{C]} \quad (3.1.2)$$

where:

- $\bar{\epsilon}^{pl}$ represents the effective plastic deformation;
- $\dot{\bar{\epsilon}}_{pl}$ – effective deformation speed;
- $\dot{\epsilon}_0$ – normal deformation speed (usually equal to 1 s⁻¹);
- n – exponent that takes into account the crumbling of the material;
- m – exponent that takes into account the melting of the material;
- T_{ref} – represents the temperature at which parameters A, B and n are determined;
- T_{solid} – the solidification temperature of the material;
- A, B, C – the material constants.

and the first factor represents the crushing of the material, the second factor represents the influence of the deformation speed, and the third factor represents the effect of temperature.

The contact law is applied to describe the shear forces between the surface of the rotating active element and the work piece. In most studies, the contact law used is the Coulomb law, because with it the best results have been obtained. This law estimates the reciprocal movement between two segments, respectively a shear contact (regardless of whether the elements stick or slide) (rel. 3.1.3) [D07, N03].

$$\tau = \mu \cdot \sigma_n \quad (3.1.3)$$

where: τ represents the tangential voltage; μ - coefficient of friction; σ_n - the voltage in the normal direction at the surface.

The equations of a thermomechanical problem can be written in two different formulations: Lagrangian and Eulerian. In the Lagrangian representation the network (discretization) is attached by points of the materials (nodes), while in the Eulerian representation the network is attached by spatial points. Consequently, during the flow of materials, in the Lagrangian representation the nodes of the network move and material points follow, while in the Eulerian representation the network is fixed [L06].

Compared to these two standard formulations the following were developed: CEL (Coupled Eulerian-Lagrangian) and ALE (Arbitrary Lagrangian-Eulerian). In models based on the flow of Lagrangian elements, the knots and particles of material become extremely distorted, and the results lose precision. In order to avoid major deformation, the adaptive ALE (Arbitrary Lagrangian-Eulerian) rediscrretization model [A04] is used, being the most viable method for modeling processes that involve a high degree of plastic deformation [M05]. In addition to ALE (Arbitrary Lagrangian-Eulerian), CEL (Coupled Eulerian-Lagrangian) has a number of advantages, with its help one can estimate the distribution of the material and the possible holes or defects in the welding seam [P07].

The generation of heat and its dispersion are points to be taken into account when designing a FSW numerical model, for results as close to reality as possible. The heat is generated by: the contact between the working material and the shoulder of the active element, the contact between the pin and the welding material, the rotational movement made by the active element in the material and by the plastic deformation of the material. The heat is dissipated in the workpiece according to the thermal conductivity coefficient of the working material. Heat losses occur through: the active element, the upper part of the workpiece, through the lower surface of the welding piece that comes into contact with the machine table and the clamps on the machine table, as well as through convective heat losses, in the surrounding atmosphere (these are considered negligible) [D07].

3.8. Methods for validating the numerical models of the FSW process

Validation of the numerical model of the FSW process using the temperature distribution in the welding seam and its evolution over time

The most accessible method of validating a numerical model is the comparison of the temperature field distribution in the welding seam obtained by simulation and its evolution over time, compared to the values recorded experimentally. Although the process temperatures are lower than the melting points of the welding materials, they are large enough to cause phase transformations. Usually, when conducting experiments, the temperature is measured by means of thermocouples [N03] or by the thermographic chamber [B07, C16, E02].

For the validation of a numerical model, the values of the recorded temperatures were used using two K-type thermocouples positioned at a depth of 1,5 mm in the material and placed at 8 mm, respectively 33 mm, compared to the beginning of the welding seam. The temperature resulted in the simulation of the numerical model is in agreement with the experimental one, the maximum difference between them being 5 °C (Fig. 3.8.2). This model is considered to be validated [R01].

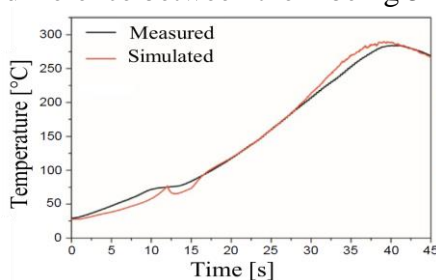


Fig. 3.8.2. Temperature distribution measured and simulated [R01]

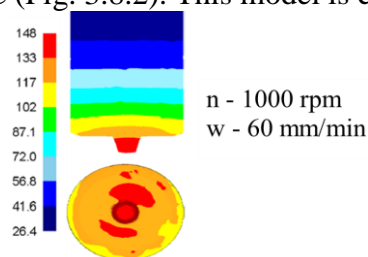


Fig. 3.8.3. Temperature distribution on the profile of the rotating active element [J01]

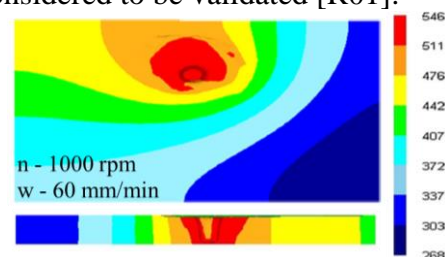


Fig. 3.8.4. Temperature distribution along the longitudinal direction of the welding seam [J01]

The maximum temperature reached during the FSW process is located in the center of the welding seam, due to the rotation and contact between the pin and the shoulder of the active element with the welding materials (Fig. 3.8.3 and 3.8.4) [J01]. Taking this into account, it can be concluded that the use of a thermographic chamber or of thermocouples may induce measurement errors attributed to the area where the recordings are made. Both the thermographic chamber and the thermocouples cannot have a direct view or a direct contact on the active element – part interface.

The temperature profile, in both longitudinal and transverse sections, has a “V” shape, this shape appears due to the shoulder diameter of the active element which is larger compared to its pin, which leads to the generation of heat on a larger surface in the upper area of the welding seam compared to the lower area. Another factor that determines the shape of the temperature distribution is the thermal transfer of heat between the weld plates and the mass of the machine, which is much higher than the heat transfer between the upper part of the welded parts and the atmosphere (Fig. 3.8.4) [J01].

Validation of the numerical model using temperature distribution is one of the most accessible methods, both from the point of view of the experiments and of the simulation.

Validation of the numerical model of the FSW process using the welded seam shape

A numerical model built respecting the input conditions of the process it simulates will be able to predict the shape of the welding seam and the possible defects for any set of parameters. The numerical model of the FSW method for the head-to-head coupling of two similar AA2024 alloys, made in software ABAQUS/ Explicit, using the CEL (Coupled Eulerian-Lagrangian) method and the Johnson-Cook and Coulomb behavior laws, was validated by comparing the presence of defects and the shape of the burrs resulting by simulation with those present on the samples made experimentally (Fig. 3.8.9 – 3.8.11). The dimensions of these defects are not identical, but their appearance due to the unpaired input parameters can be highlighted by numerical simulation. This allows the optimization of the parameters and the reduction of the costs with the experiments by the appropriate choice of the input parameters [S03].

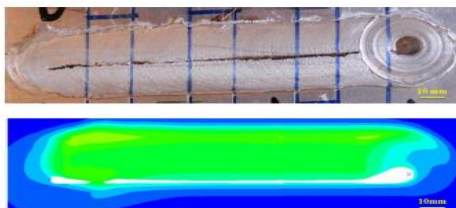


Fig. 3.8.9. Channel type defect: experimentally and simulated [S03]

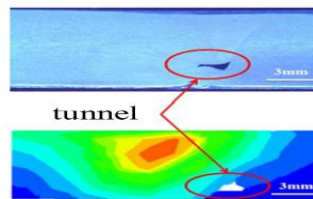


Fig. 3.8.10. Tunnel defect: experimentally and simulated [S03]

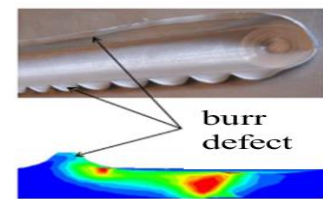


Fig. 3.8.11. Burr defect: experimentally and simulated [S03]

3.9. Results of the simulation of the FSW process of structures of different materials

In the studied literature we have found a small number of papers presenting the numerical modeling of the FSW process for different materials. The small number of works can be justified by the difficulty of articulating the characteristics of several materials in the working system.

One of the few works presenting the steps to perform the simulation of FSW jointing of two different materials is based on two different aluminum alloys: AA5083 and AA6061 [A04]. Numerical modeling was performed in the ABAQUS software, using the CEL (Coupled Eulerian-Lagrangian) technique. The welding speed is defined as an entry within the limit of the Eulerian domain, which has a dimension considered to be four times the diameter of the active element's shoulder, a cubic shape and is divided into three zones: hollow (1 mm high), piece 1 and piece 2.

The active rotating work element is designed to be Lagrangian rigid, and the interaction between it and the work parts is realized with the Coulomb friction law using an explicit contact. The behavior of materials in the plastic field is defined by the Johnson-Cook law. The welding phase is simulated using volume deformation. The material flow simulates the advancement of the active element along the joining area [A04]. Input parameters are: penetration speed 100 mm/min, rotation speed 900 rpm, welding speed 50 mm/min and tilt angle 2°.

The Eulerian domain consists of 82800 discretization elements with 8 nodes, each element has 4 degrees of freedom for each node (EC3D8RT) [A04].

The numerical model validation was performed by comparing the temperatures obtained by simulation with those determined experimentally [A04]. Temperatures were measured 10 mm from the median plane of the welding seam on both materials, on the advance and the retraction side. Between the values obtained by simulation and those measured, there is a difference of 8 – 15 %, a difference given largely by the inaccuracy of the temperature measurement and recording system (Fig. 3.9.2).

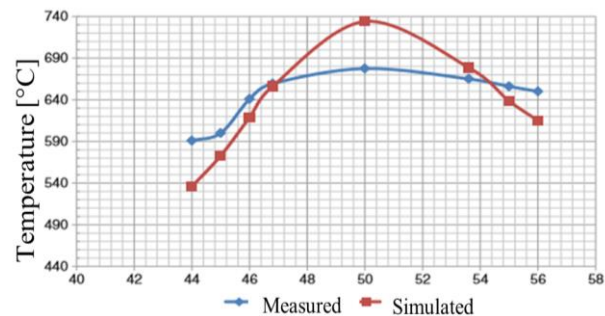


Fig. 3.9.2. Temperature history, 10 mm from the center of the welding seam, on the feed side [A04]

The numerical simulation can successfully replace the experimental part, in terms of the costs and resources allocated for carrying out the experimental studies. However, the simulation has a disadvantage, respectively the very long processing time of the data in order to obtain correct results.

Chapter 4. Conclusions on the current state of research – development and industrial applications of friction stir welding with rotating active element

From the analysis of the current state of research – development and industrial applications of friction stir welding with rotating active element, important conclusions are drawn, as follows:

- The friction stir welding process (FSW) is considered as one of the most significant welding achievements of the last period. It was invented in 1991 in the United Kingdom at the Welding Institute (TWI) (s. § 1.1). Initially it was developed for welding aluminum alloy plates, and over time the studies expanded to welding materials such as polymeric materials, metallic materials – brass, copper, magnesium, titanium, steel – and composite materials with aluminum metallic matrix, copper and titanium, and ceramic reinforcement from particles such as Al_2O_3 , SiC, Si_3N_4 și B_4C (s. § 1.5.1).
- The working principle of the FSW process is simple: a rotating active element, with a rotational movement and a translational one penetrates the material, in the area of the welding joint, moves along it and exits the material at the end of the welding seam. The technological parameters of the process are: rotation speed [rpm], welding speed [mm/min] and the inclination angle of the active element (s. § 1.3).
- Most of the studies performed to date have been developed for welding aluminum alloys from all eight groups, the studies focusing on alloys that are impossible to weld using classical procedures. The multitude of existing studies presents various combinations of two aluminum alloys, both identical and different, positioned end to end or superimposed, using a diverse range of input parameters and active elements. So far, no study from the analyzed ones has focused on the use of the FSW process for the joining of three different aluminum alloys (s. § 1.5.2).
- The rotating active element used to make the FSW plays three main roles: it warms up the workpieces, mixes the laminated material after the heating, controls and restricts the movement of the processed material in the upper area, using its shoulder. The important features of the active working element are the shape, dimensions and properties of the material from which it is made (s. § 1.6).

- The patents and licenses obtained for the FSW process were oriented to the following sectors of development: the auto industry, the aeronautical and aerospace industry, the railway industry, the naval industry, the metalworking, research and development and others. The countries using this process on an industrial scale are: United Kingdom (the country where the process was invented), USA, Canada, Japan and China (s. § 1.8.1).
- The active parts of the rotating element are: its shoulder, which comes into contact with the welding material and the pin, which penetrates the welding material. The size and shape of the shoulder of the active element influences the temperature and material distribution on the surface of the welding seam, and the pin of the active element produces deformation of the material and its heating inside the welding seam, moving the material in front of the active element behind it. The shapes and dimensions of the active element are varied, but for the welding of aluminum alloys the best results were obtained using a rotating active element with cylindrical or conical pin, threaded and concave shoulder (s. § 1.6).
- The use of FSW in the aeronautical industry is most widespread for two reasons: this process is heavily researched and operated for welding different aluminium alloys, and the fuselage of an aircraft consists of 20 – 50 % aluminium alloys which are currently joined by rivets. The most common alloys used in the aviation industry are: AA6061, AA2024 and AA7075. Not all of the three can be welded using conventional procedures, but all can be welded using the FSW process (s. § 1.8.2).
- Currently, the FSW process is used in the aeronautical industry for the manufacture of: fuselages, cryogenic fuel tanks for spacecraft, aviation fuel tanks, military aircraft tanks, military and scientific missiles (s. § 1.8.2).
- The automotive industry aims to reduce the weight and increase the resistance of standard vehicles, this can be achieved by combining alloys from different aluminum series using the FSW welding process. Currently, this process is used in the mass production by Mazda Motor, in the construction of the hood and the boot for the Mazda RX-8 sports model, in the rear doors for the Mazda MX-5, in the suspension and in the assembly of the covers for door handles on certain Ford models. Also, FSW is being evaluated for the following potential applications at industrial area: engine and chassis construction, aluminum rims, piping, truck bodies, truck cranes, mobile cranes, fuel tankers, the realization of the fuel tanks, the realization of the personalized space from caravans, the realization of certain components of the buses and the vehicles of public transport, the realization of the truck etc. (s. § 1.8.3).
- Other areas, where the FSW process has entered, are the shipping and maritime industries for the following applications: decks, walls and floors, aluminum extruded, boat sections, superstructures, helicopter landing platforms, masts and arms, for example for sailboats, refrigeration installations; in the railway industry it is used for: railway rolling stock, subway cars, trams, railway tanks and freight wagons, container bodies; The electrical industry shows increasing interest in applications such as: electric motor housings, electrical connectors, electronic encapsulation. FSW can also be considered for: refrigeration panels, cooking equipment and kitchens, gas tanks and gas cylinders, connecting copper or aluminum coils, furniture, aluminum bridges, aluminum facade panels, copper or titanium, window frames, aluminum pipes etc. (s. § 1.8.4).
- The quality level of welding seam made using the FSW process can be controlled visually, dimensionally or by testing, and the quality indicators of these welding seam are: microstructure of welded joints, precipitation state in welding seam, texture of welded joints, the remaining tensions in the welding seam, the lack of defects inside the welding seam, the microhardness, the tensile strength and the ductility (s. § 2.1).

- From a macrostructural point of view, the FSW welding seam is divided into 4 distinct areas: the base material at the greatest distance from the center of the welding seam (BM), the affected zone thermally influenced by the thermal cycle at the time of the process (HAZ), the zone thermally and mechanically affected where the material is plastic deformed by the active element and thermally affected by the heat released during the process (TMAZ) and the welding zone, represented by the area where the pin of the working active element penetrates (WZ) (s. § 2.2.1).
- The way of mixing the materials and the macrostructure of the joint are influenced by the shape and size of the active element, the values of the technological parameters of the process and the position of the materials to be combined with each other. Thus, the volume of the mixed material increases inversely proportional to the feed rate, the core of the welding seam being dominated by the material placed on the forward side of the active element, so that the placement of the softer material on the withdrawal side of the active element is indicated, and the core of the welding seam welding is mainly oriented towards the withdrawal zone of the active element. The shape of the section of the welding seam and the way of distribution of the four characteristic areas can generate information regarding the efficiency of the working regime, the correctness of the chosen active element and the mechanical properties of the joint (s. § 2.2.1).
- The microstructure of the FSW joint is directly dependent on the shape and distribution of the four macrostructural areas of the welding seam. There was a refining of the grains as the distance decreased relative to the core of the welding seam, grains having a major plastic deformation, being formed predominantly from the alloy positioned on the feed side of the active element. The shape and size of the grain in the WZ greatly improve the mechanical properties of the welding seam (s. § 2.2.2).
- The FSW welding process significantly changes the microstructure of the joint, in terms of the grain size and the orientation of the precipitate layer (these can be completely or partially redissolved during the process). The precipitates present in different areas of the welding seam obviously depend on the initial composition of the basic materials, the heat flow determined by the welding conditions and their position in the section of the welding seam. The density of the precipitates is higher in the HAZ area than in the WZ or TMAZ, because the material in this area is exposed only at high temperature, without being mechanically affected, so that the precipitate dissolution is insufficient (s. § 2.2.3).
- The remaining stresses related to the FSW process can be of two types: transverse (perpendicular to the welding direction) and longitudinal (parallel to the welding direction). These are influenced by the technological parameters and it has been shown that longitudinal stresses increase with increasing feed rate. The highest residual stresses appear longitudinally, on the forward side of the rotating active element and have a strong influence on the mechanical properties of the joint (s. § 2.2.5).
- The defects in the FSW welding seam are different from the defects recorded in the classical procedures. These can be in appearance: jagged seam, scales, burrs, crack along the welding seam, uneven seam or defects in the macrostructure of the welding seam: tunnel or "wormhole" defects, collapsed core defect, defect due to the "*lack of penetration*" and defect of type "*kissing bond*". When carrying out the FSW process, the technological parameters can lead to the appearance of defects if they are not chosen properly. Another factor of appearance of defects is the contrast of the properties of the materials in the case of joining different materials. Defects can be prevented by improving the heat input into the welding area and controlling it during the process (s. § 2.3).

- The values of the microhardnesses in the FSW joint give an indication of the phase change and the granulation size in the section of the welding seam, which may increase in the areas with finer particles homogeneously distributed, respectively, in the area of the welding core. The microhardness of the welding seam is influenced both by the technological parameters, increasing directly proportional to the feed rate, the shape of the active element used, as well as the values of the microhardness of the basic materials. For the experiments in which two different aluminum alloys are welded with large differences of the microhardnesses of the basic materials, the final microhardness of the welding seam can be negatively influenced by the material with the lowest microhardness (s. § 2.4.1).
- The tensile strength of the FSW joint has been shown to decrease with respect to the base material, representing about 70 % of the value of the base material. According to the studies, it has been shown that the value of the mechanical strength increases directly in proportion to the feed rate, and from the point of view of the active element used the best results were obtained for the one with the threaded cylindrical pin (s. § 2.4.2).
- Numerical simulation is a powerful tool for understanding the phenomena that operate during the FSW welding process. The development of a numerical model corresponding to the FSW process represents a great challenge for any researcher due to its complexity and the fact that the working principle of the process leads to large deformations that occur during the joint. With the help of numerical simulation it is possible to visualize and analyze the material flow, temperature range, stresses and deformations involved, and these can be obtained with greater ease than by the experimental methods. In most of the cases studied, the main research topic was the evaluation of the temperature field, these being large enough to lead to phase transformations in the material (s. § 3.1).
- The steps of realizing a numerical model corresponding to the friction stir welding process by rotating active element are the following: defining the geometry of the piece and the active welding element, defining the behavior of the material (elasto-plastic or elasto-viscoplastic) by a law of behavior, defining the elastic and physical properties and the heat transfer, defining the type of contact between surfaces and the friction law, establishing the boundary conditions and process parameters, discretizing the rotating active element and the welding parts (s. § 3.1).
- When designing the numerical model corresponding to the FSW process, the shape, dimensions and location in the working system must be taken into account, both for the parts to be welded and for the active element. It is necessary that they correspond to reality in order to obtain the most relevant result (s. § 3.2).
- In most studies, the law of behavior of materials for defining the constructive mathematical model used in numerical simulation is Johnson-Cook, because, in general, the behavior is viscous-plastic (s. § 3.3), and the law of contact applied to describes the shear forces between the surface of the active element and the workpiece is defined by the Coulomb law, because it estimates the reciprocal movement between two segments, regardless of whether they stick or slide (s. § 3.5). The equation for defining the thermomechanical behavior of the materials, which offers the most advantages and is most often used when developing a numerical model for the FSW process, is the CEL (Coupled Eulerian-Lagrangian). With this help one can estimate the distributions of the material and the possible holes/ defects in the welding seam (s. § 3.1).
- The dimension of the discretization elements has a strong influence on the quality of the results recorded by the numerical model realized. A network of large elements cannot produce sufficiently precise results, while a network of smaller elements can be very expensive in terms of simulation time. The compromise variant used is represented by the partitioning of the joining plates and the realization of the discretization elements with different dimensions depending on their position in the working system (s. § 3.7).

- Another important step in the development of a numerical model is its validation. The validation consists in comparing the simulation output data with the experimental study data, both performed under identical conditions. Different criteria can be used to validate the numerical model, such as: the temperature distribution in the welding seam and its evolution over time (method most frequently used), the distribution of residual stresses, the axial force and the torque applied to the active element in the process time, the shape of the welding seam, the microhardness measured in different areas and its evolution, with the help of viscosity (s. § 3.8).
- In the studied literature we found a relatively small number of papers presenting the numerical modeling of the FSW process for different materials. The small number of works can be justified by the difficulty of attributing the characteristics of several materials in the working system (s. § 3.9).

Part II.

**Contributions to the theoretical – experimental
research and numerical modeling on
the process and system of friction stir welding
with rotating active element
of different aluminium alloy structures**

Chapter 5. The directions, the main objective and the research - development methodology regarding the friction stir welding of different aluminum alloy structures

5.1. Research - development directions

Based on the analysis of the current stage, the following directions of research - development are considered to be topical on processes and systems of friction stir welding with rotating active element of structures of different materials:

- increasing the range of different industrial materials joined by friction stir welding with rotating active element;
- diversification of the joint structures by means of friction welding procedures with an active rotating element, by increasing their complexity;
- developing the knowledge regarding the phenomena that occur during the friction stir welding process, with establishing the influence that different parameters have on the process and the characteristics of the joint structure;
- development of numerical models for simulating FSW welding processes, using different techniques, to allow the welding process to be optimized.

5.2. The main objective of the research - development activity

Taking into account the data and conclusions drawn from the analysis of the current stage, as well as the research - development directions regarding the processes and systems of friction stir welding with rotating active element, it is determined as the main objective of the research - development activity in the doctorate: **process and system development of friction stir welding of different aluminum alloy structures, through theoretical - experimental research and numerical modeling.**

The structures of different aluminum alloys are obtained by joining three overlapping plates, the aluminum alloys are AA2024, AA6061 and AA7075, they have different chemical and mechanical properties and are frequently used in the aeronautical industry, in aircraft construction.

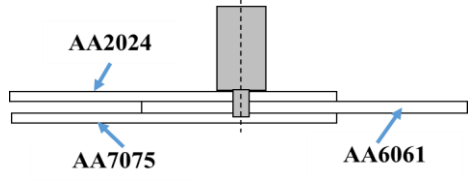
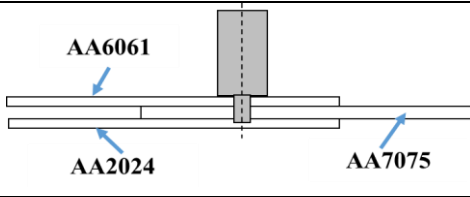
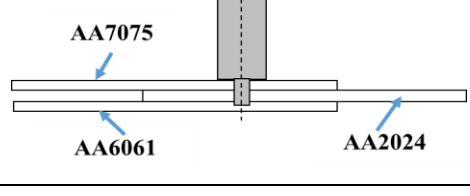
Experiment planning

When planning experiments, the following must be achieved: setting the limits, number, values and combinations of values of the independent variables [U01].

In relation to *the position of the component plates in the welding structure*, in the preliminary investigations, three of the six possible positions were investigated, respectively (Table 5.3.3): AA2024 – AA6061 – AA7075, AA6061 – AA7075 – AA2024 and AA7075 – AA2024 – AA6061. In the advanced research, only the positioning of AA7075 in the upper part, AA2024 in the middle part and AA6061 in the bottom of the structure was used, because for this positioning of the plates have been obtained, in the preliminary research, corresponding characteristics of the joint.

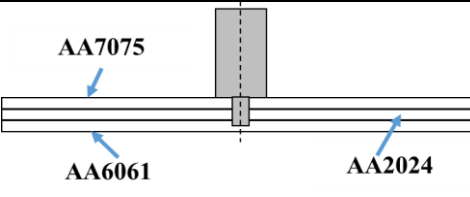
For the realization of the experimental plan related to the preliminary researches, for each positioning of the aluminum alloy plates, a complete factorial plan with two levels and two repetitions at the center was applied, respectively, with a total number of six experiences for each positioning of the aluminum plates other aluminum (Table 5.3.3).

Table 5.3.3. Planning of preliminary experiments

Welded structure code	The position of the component plates of the welded structure	Exp. no.	Exp. code	Standard independent variables		Natural independent variable	
				Rotation speed, n	Welding speed, w	Rotation speed, n [rpm]	Welding speed, w [mm/min]
Structure 1		1	1.1	-1	-1	600	70
		2	1.2	1	-1	1400	70
		3	1.3	-1	1	600	170
		4	1.4	1	1	1400	170
		5	1.5	0	0	1000	120
		6	1.6	0	0	1000	120
Structure 2		7	2.1	-1	-1	600	70
		8	2.2	1	-1	1400	70
		9	2.3	-1	1	600	170
		10	2.4	1	1	1400	170
		11	2.5	0	0	1000	120
		12	2.6	0	0	1000	120
Structure 3		13	3.1	-1	-1	600	70
		14	3.2	1	-1	1400	70
		15	3.3	-1	1	600	170
		16	3.4	1	1	1400	170
		17	3.5	0	0	1000	120
		18	3.6	0	0	1000	120

Similarly, a complete factorial plan with two levels and two repetitions at the center was applied to the elaboration of the experimental plan related to the advanced research (Table 5.3.4).

Table 5.3.4. Planning of advanced experiments

Welded structure code	The position of the component plates of the welded structure	Exp. no.	Exp. code	Standard independent variables		Natural independent variable	
				Rotation speed, n	Welding speed, w	Rotation speed, n [rpm]	Welding speed, w [mm/min]
Structure 4		19	4.1	-1	-1	650	60
		20	4.2	1	-1	1100	60
		21	4.3	-1	1	650	100
		22	4.4	1	1	1100	100
		23	4.5	0	0	845	80
		24	4.6	0	0	845	80

Planning the development of the numerical model

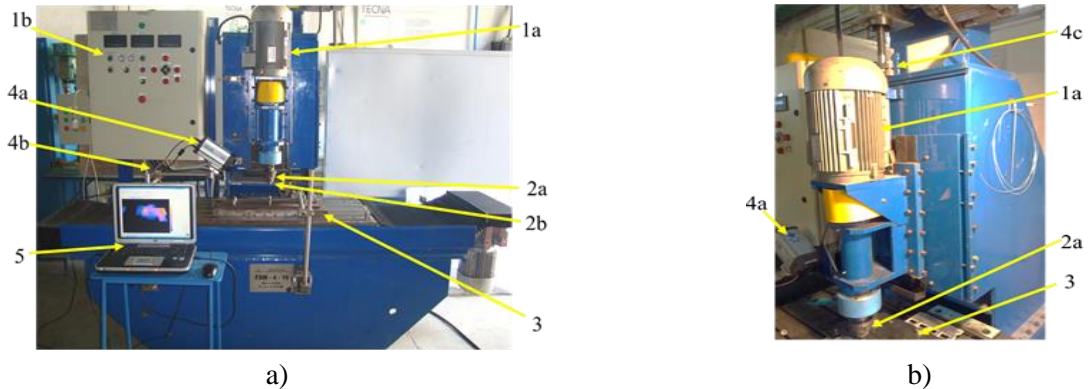
For numerical modeling of the FSW process, the software ABAQUS 6.13/ Explicit will be used because, on the one hand, it is available in the Manufacturing Laboratory at the University of Pitesti and, on the other hand, it is one commonly used for the simulation by the element method finished FSW processes [B07].

The technique for realizing the numerical model is adopted to be the CEL (Coupled Eulerian-Lagrangian), because it can estimate the large deformations, the distribution of the material and the possible gaps or other defects generated along the welding seam during the FSW process (v. § 3.1). Thus, the numerical model will have the geometrical characteristics of the rotating active element and the properties of the three materials, and the positioning of the aluminum alloy plates in the joint structure will be identical to the position used in the experimental researches. The values of the technological parameters will be those for which, in the experimental researches, a flawless welding seam with corresponding mechanical properties was obtained.

Capitolul 6. Elements of the experimental research system for the friction stir welding of different aluminum alloys structures

6.2. The experimental stand and the process characteristics measured in real time

The experimental stand consists of the FSW 4-10 welding machine, the device for orientation and fixing of the welding parts, the active rotating welding element, the fastening device for the welding rotating active element and the system for acquiring, monitoring and recording the data generated in during the welding process (Fig. 6.2.1) [B07, B10, B11, B12, G06].



- 1a – Motor and shaft of FSW 4-10 machine;
- 1b – Control panel of FSW 4-10 machine;
- 2a, b – Clamping device (a) of the active rotating welding element (b);
- 3 – Device for fixing and orienting welding parts;
- 4a, b – FLIR A40M infrared thermographic camera (a) and manipulator for fixing and adjusting the camera in working position (b);
- 4c – Force sensor with AM type transducer (0 – 20 kN);
- 5 – Laptop used for data acquisition.

Fig. 6.2.1. The experimental stand: a) frontal view; b) side view

The device for orientation and fixing of welding parts, designed and manufactured to facilitate the orientation and fast fixing of welding parts.

The FSW process is continuously monitored during performing the welding seam. The process characteristics recorded during the welding process are: the process temperature, in the joint area, and the axial force of the process, respectively, the force exerted on the rotating rotating active element of welding after the direction of the axis of rotation.

The process temperature is measured by the infrared thermographic chamber FLIR A40M. The thermographic chamber was positioned in the working system (Fig. 6.2.4) [B06, B07, B11, B12] and adjusted so as to measure and record the temperature immediately behind the rotating active element, in the middle of the welding seam.

The axial process force was measured using a sensor with the WIKA compression force transducer, model F1211, with the working range 0 – 20 kN and the relative linearity error $\pm 0.3\%$ F_{nom} positioned on the main axis of the FSW welding machine (Fig. 6.2.7) [B11].



Fig. 6.2.4. Position of the thermographic chamber within the experimental stand



Fig. 6.2.7. Position of the force sensor in the experimental stand

6.3. Welding rotating active element

The geometry of the welding rotating active element is of major importance in the FSW process. This should be chosen so that during the process the active element is thermally efficient and leads to the most effective mixing between the joining materials. Also, the material from which it is made must have high hardness and high temperature resistance (Fig. 6.3.1).

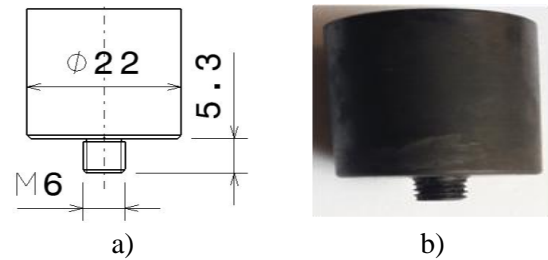


Fig. 6.3.1. Used rotating active element

6.4. Defining and production of welding parts

All experiments were performed using pieces taken from a single batch of material, for each individual alloy. The pieces used in the preliminary experiments are identical for all three alloys, with dimensions of 250 x 140 x 2 mm. For the advanced experiment it was decided to increase the dimension from 140 mm to 200 mm. In making the joints, the direction of lamination of the plates was taken into account, so that it is parallel to the direction of the welding seam.

It is noted that the cutting of sheets of sheet, according to the drawing schemes, was done with guillotine so as not to thermally affect the specimens.

6.5. Defining and sampling of the sample for characterisation of joint made

The following conditions were taken into account when carrying out the test cutting scheme:

- the cutting of the specimens should be at least 50 mm from the starting point of the seam, because that area is relatively unstable;
- the specimens to a given analysis are 2 -3 parts, from different areas of the welded structure/ welding seam to highlight the effect of stabilizing the process on the characteristics of the joint;
- each specimen, defined transversely on the welding seam, shall include a median part of the weld seam.

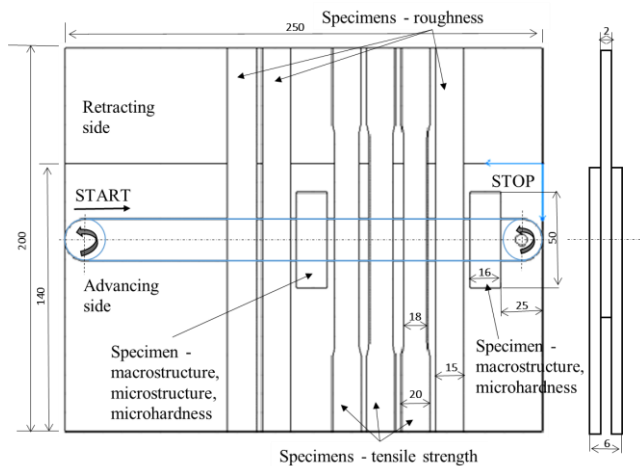


Fig. 6.5.1. Characteristics of specimens defined within each preliminary welded structure

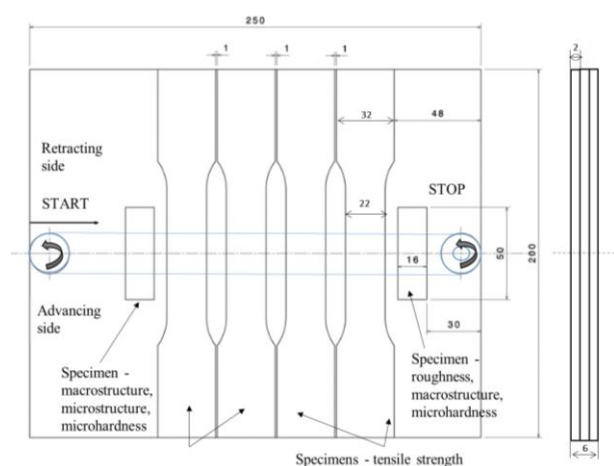


Fig. 6.5.2. Characteristics of specimens defined within each advanced welded structure

The specimens made in the preliminary experiments were taken in accordance with the dimensions recommended in the standards specific or/and in the specialized works studied [S18, S19] (v. și § 2.2 și 2.4) as presented in the Fig. 6.5.1. In preliminary research, the preparation of the tensile test system found that complex special elements were required for the orientation and fixing of specific specimens.

The shape and dimensions of the advanced welded structures are as shown in Table 5.3.4, and the shape, some dimensions, position and number of specimens defined and used within each advanced welded structure are as shown in Fig. 6.5.2 [C17, G06].

The cutting of the specimens from the joint plates was performed on a numerically controlled water jet cutting machine, in order not to affect the properties of the welding seam.

6.7. Preparation of specimens

Preparation of specific specimens for macroscopic, microscopic and microhardness analysis

The polishing of the specimens was made with metallographic paper covered with silicon carbide particles of 5 different granulations, used in descending order until a satisfactory result was obtained (from P320 to P3000). The metallographic paper used is standardised according to the FEPA (Federation of European Producers of Abrasives) scale, which is mainly used in Europe.



Fig. 6.7.2. Minitech 263 two-plate grinding machine

The polishing was done after the sanding operation, its purpose being to make a flat surface with a gloss. The polishing was done on the same machine as the sanding Minitech 263 (Fig. 6.7.2), and the metallographic paper was replaced with deer skin and alumina polishing agent (Al_2O_3) with fineness degree 3.

The chemical attack was made after polishing and polishing, the main purpose of this operation being to highlight the structural constituents of the three alloys for the macrostructural and microstructural analysis of the welding seam. The reagent used was hydrofluoric acid (HF), applied by buffering for 15 – 20 seconds, after which the sample was washed under running water until it lost its luster and became matte.

Preparation of specific specimens for the tensile test

The samples used to determine the tensile strength of the structures realized in the advanced researches, *dumbbell* type, are in number of four for each experiment (v. § 6.5 și Fig. 6.7.4) was been milled on both sides, respectively, at a width of the calibrated area of 15 mm (Fig. 6.7.5), so that the shape and dimensions comply with the provisions of SR EN ISO 6892-1 [S18].

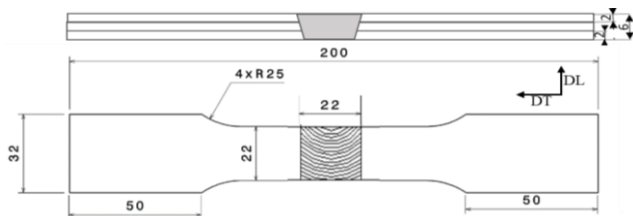


Fig. 6.7.4. Form and dimensions of specimen used to determine tensile strength before processing for advanced experiments

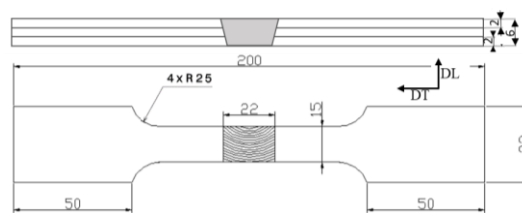


Fig. 6.7.5. Form and dimensions of specimen used to determine tensile strength after processing for advanced research

The specimens used in the tensile tests for which the DIC, (Digital Image Correlation) [C17, S20] was used required additional training consisting of: polishing the surface of interest with abrasive paper; surface cleaning with acetone; delimiting the area of interest; painting the surface in white with matte paint; use of a black paint to spray the surface of interest in order to create *freckle points* (trough contrast); detaching the adhesive tape without damaging the encoded surface.

6.8. Measuring the roughness of the welding seam

For determine the roughness values was used the roughness meter digital, portable, type MAHR PS-10 (Fig. 6.8.1). The sample for measuring the roughness of the welding seam have been defined, taken from three specific areas - and prepared as shown in § 6.5, § 6.6 and § 6.7.1. Basically, three roughness values were recorded from each sample/ area.



Fig. 6.8.1. MAHR type PS-10 rugosimeter

6.9. Macroscopic and microscopic analysis

The macroscopic analysis was performed using a metallographic microscope of the type OPTIKA ITALY (Fig. 6.9.1), and the microscopic analysis – with a metallographic microscope adapted for the examination of metals, with a magnification capacity of up to 500X, of the type OLYMPUS BX51M (Fig. 6.9.2)



Fig. 6.9.1. Metallographic microscope OPTIKA ITALY



Fig. 6.9.2. OLYMPUS BX51M metallographic microscope

6.10. Measurement of microhardness

For measuring and analyzing the microhardness the Vickers method was used [V03]. The determinations were made on a machine of the type INNOVATEST FALCON 500 (Fig. 6.10.1).

The values of micro-hardness were determined in cross-section, with a load of 2,94 N (300 g) and a penetration duration of 10 seconds. The microhardness profile is obtained by measurements made in 33 points arranged on three separate subsidiaries, corresponding to each piece in the welded structure. Each branch comprises 11 points positioned at a distance of 1 mm between them and symmetrical to the center of the welding seam.



Fig. 6.10.1. INNOVATEST FALCON 500 microdurimeter

6.11. Measurement of tensile strength

Traction tests were performed within ENSTA Bretagne, used a hydraulic machine, of the type INSTRON 1342, with a capacity of 100 kN (Fig. 6.11.1) [C17, G06]. WaveMatrix (Instron) software was used to schedule input data and work activities, as well as to record output data.

For measuring the displacement and deformation field (elongations and relative elongations), the DIC (Digital Image Correlation) method was used [S20] which is a contactless optical measurement method (Fig. 6.11.2).



Fig. 6.11.1. INSTRON 1342 tensile test machine for traction/compression

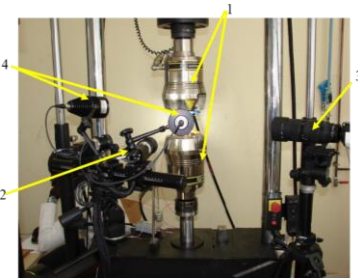


Fig. 6.11.2. Work system for tensile testing and DIC (Digital Image Correlation)

Chapter 7. Results of the preliminary theoretical - experimental research on the friction stir welding process and system of different aluminum alloys structures

Results of the preliminary theoretical - experimental research regarding system and process of the friction stir welding of different aluminum alloy structures, which also include published elements of the author [B06, B10, B11, B12], are presented below, grouped by the dimensions analyzed during the research.

7.1. Process temperature

Process temperature is an important feature of the FSW welding process (v. § 5.3.1). The temperature in the welding zone was measured during the working process – the penetration phase and, the welding phase along the welding seam, as presented in sub-chapter 6.2.

Based on the characteristics of the process temperature evolution, the average process temperature in the welding zone/ phase, T_{med} , can be determined (Table 7.1.1 and Fig. 7.1.6).

Table 7.1.1. Values of the average temperature in the welding area / phase

Exp. type	Technological parametres		T_{med} [°C]		
	n [rpm]	w [mm/min]	Structure 1	Structure 2	Structure 3
1	600	70	397	455	506
2	1400	70	465	505	543
3	600	170	362	441	520
4	1400	170	371	494	550
5	1000	120	345	468	524
6	1000	120	419	481	539

The analysis of temperature and average temperature evolution (Table 7.1.1 and Fig. 7.1.6) during the welding process reveals a series of dependencies. The following are highlighted.

- The process temperature is directly influenced by the joint structure, by the characteristics of the aluminum alloy positioned at the top of the structure, respectively, at the same values of the technological parameters n and w : structure 1, at which the alloy with the minimum melting temperature is positioned at the top, AA2024, generates minimum process temperatures; structure 2, at which the upper melting alloy, AA6061, is positioned at the top, generating average process temperatures; structure 3, at which the alloy with the maximum melting temperature, AA7075, is positioned at the top, generating maximum process temperatures [B10];

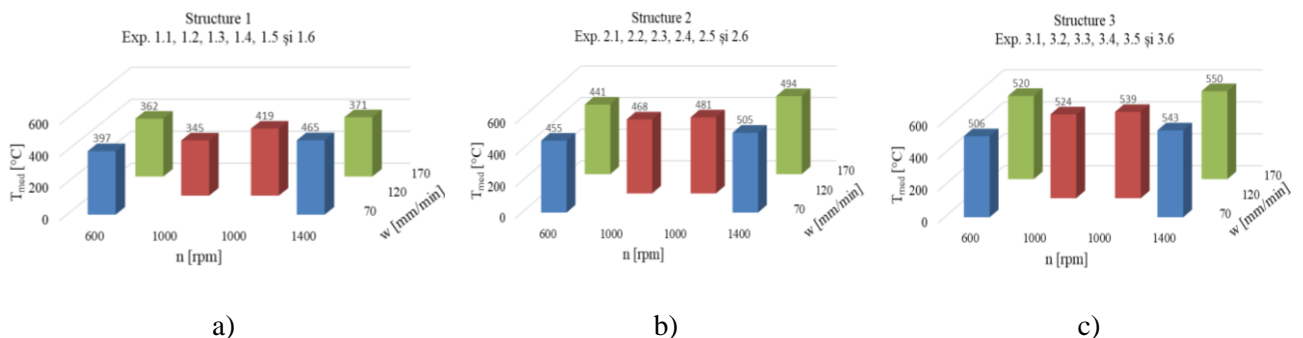


Fig. 7.1.6. The average process temperature in the welding zone/ phase, T_{med} , depending on n and w

- The rotation speed directly influences the process temperature (Table 7.1.1 and Fig. 7.1.6) [B06, B11, B12];
- The welding speed has a small influence on the process temperature, in correlation with the properties of the alloy positioned at the top of the analyzed structure. Thus, for structure 1 – AA2024 in the upper part and structure 2 – AA6061 in the upper part, the increase of the feed rate generates a decrease of the average temperature in the welding zone/ phase, and for the structure 3 – AA7075 in the upper part, the increase of the feed rate, it generates a very small increase of the average temperature in the welding zone/ phase (Table 7.1.1 and Fig. 7.1.6).

7.2. Axial process force

The axial process force, respectively, the force exerted on the rotating active element in the welding process, is an important feature of the FSW welding process (v. § 5.3.1). The axial process force was measured during the working process – the penetration phase and the welding phase along the welding seam, as presented in sub-chapter 6.2.

Based on the characteristics of the evolution of the axial process force, the following sizes can be associated:

$F_{a \max-p}$ - the maximum value of the axial force characteristic of the penetration phase;

$F_{a \max-s}$ - the maximum value of the axial force characteristic of the welding phase;

$F_{a \text{ med-s}}$ - the average value of the axial force characteristic of the stabilized welding area;

d_s - the longitudinal distance from the starting point of the welding seam, until the axial force/ process stabilization.

The values of these sizes, for the 18 experiences of the preliminary research program, are presented in Table 7.2.1 and, as the case may be, in Fig. 7.2.6 – 7.2.9.

Table 7.2.1. Values of the specific quantities associated with the axial process force

Exp. type	Technological parametres		$F_{a \max-p}$ [kN]			$F_{a \max-s}$ [kN]			$F_{a \text{ med-s}}$ [kN]			d_s [mm]		
			Structure			Structure			Structure			Structure		
	n [rpm]	w [mm/min]	1	2	3	1	2	3	1	2	3	1	2	3
1	600	70	14	16	12,3	14	9,1	12	12,5	8,9	11,5	41	53	53
2	1400	70	11,6	8	11	12,8	8,2	10,5	9,5	7,3	9,9	41	30	25
3	600	170	14,6	16	14,7	11,8	12	15,8	11,2	10,9	15,2	-	157	100
4	1400	170	11,7	11,6	12,5	10,8	12,1	11,7	10,2	10,7	11,4	120	-	10
5	1000	120	11,8	10	12	11,8	9,3	11	11	9,2	10,7	28	18	78
6	1000	120	14,3	11	13	13	10,8	13,8	12,4	9,9	13,2	38	38	88

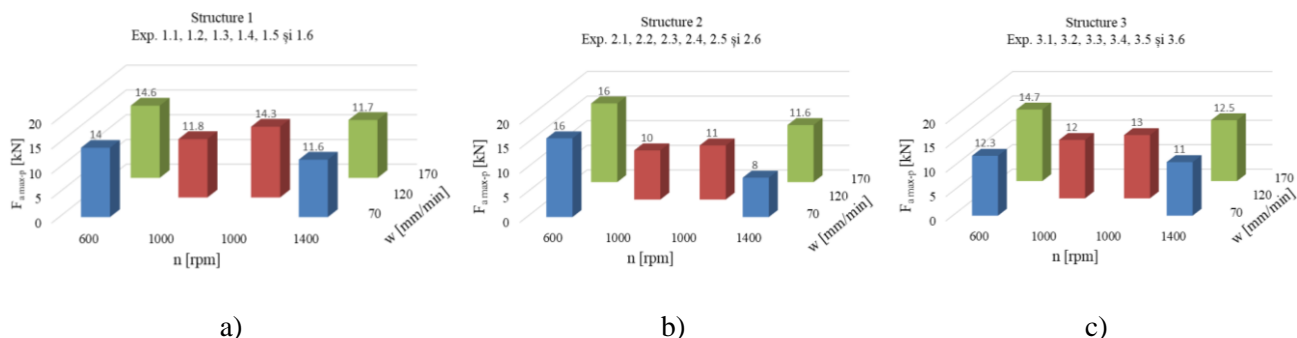


Fig. 7.2.6. The maximum value of the axial force characteristic of the penetration phase, $F_{a \max-p}$, depending on n and w

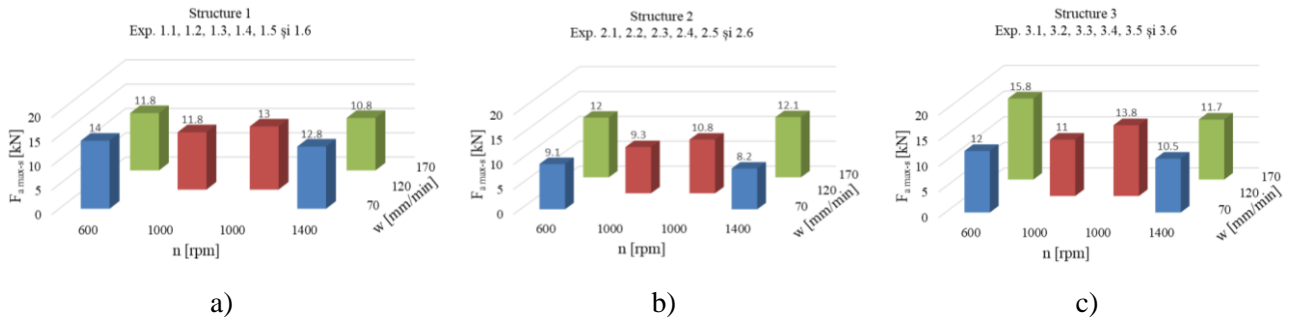


Fig. 7.2.7. The maximum value of the axial force characteristic of the welding phase, $F_{a\max-s}$, depending on n and w

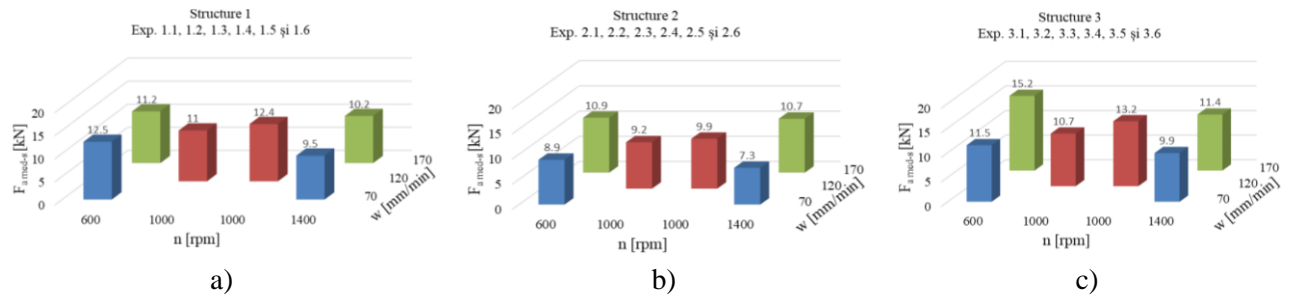


Fig. 7.2.8. The average value of the axial force characteristic of the stabilized welding area, $F_{a\text{med-s}}$, depending on n and w

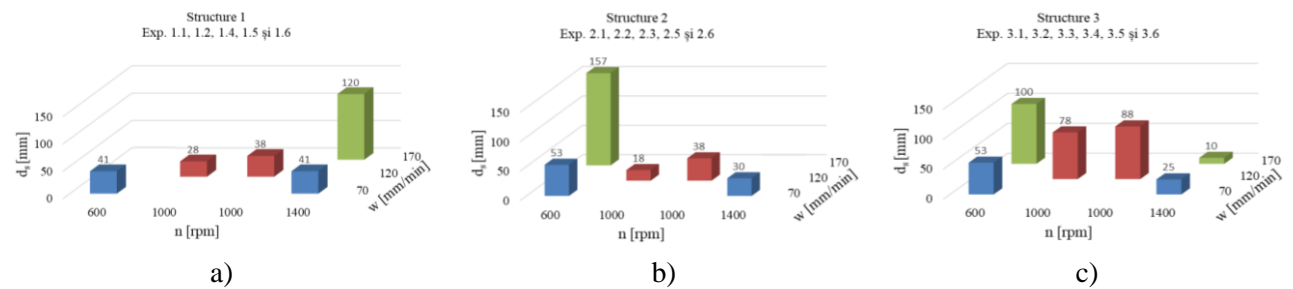


Fig. 7.2.9. The longitudinal distance until the axial force/ process stabilization, d_s , in according to n and w

The analysis of the above data highlights a series of dependencies. The following are highlighted.

- The rotation speed influences inversely the axial process force, respectively, the maximum and average axial forces in the welding area (Table 7.2.1, Fig. 7.2.6 – 7.2.8) [B11, B12];
- The welding speed directly influences the values of the axial process forces [B11]. An exception is structure 1, where, in the welding phase, the axial force shows a decrease for a certain combination of parameters (Table 7.2.1, Fig. 7.2.6 – 7.2.8). The decrease of the axial force can be favored by the degree of malleability of the material positioned in the upper area of the welding seam ;
- The distance d_s is influenced by the retention period of the rotating active element in the material penetration phase and the welding speed. Maintaining the active element during the penetration period for a longer time leads to faster stabilization of the process (Table 7.2.1 and Fig. 7.2.9) and, similarly, the decrease of the welding speed. These influences are justified by the fact that both the increase of the retention period of the rotating active element and the decrease of the welding speed result in a faster increase of the temperature at the beginning of the process, respectively, its faster stabilization.

7.3. The roughness of the welding seam

The roughness of the welding seam, an important feature of it, was measured as presented in subchapter 6.8, respectively, in three specific areas of the welded structure, for all 18 preliminary experiences. Dependence of the average value of the roughness R_a on the position of the specimen on the welding seam and on the technological parameters, for each joint structure is presented, as the case may be, in Fig. 7.3.2, 7.3.4 and 7.3.6.

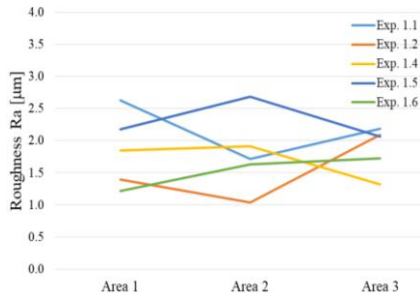


Fig. 7.3.2. Average values of roughness at structure 1

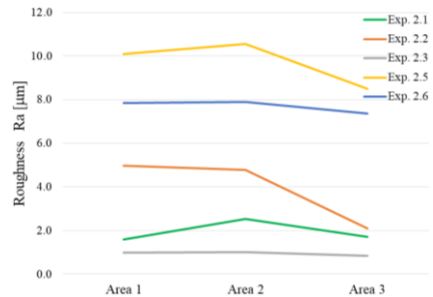


Fig. 7.3.4. Average values of roughness at structure 2

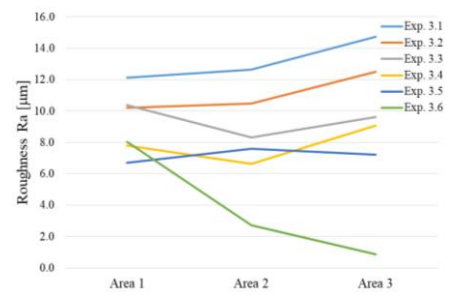


Fig. 7.3.6. Average values of roughness at structure 3

It is found that the measured roughness is influenced by the nature of the material positioned in contact with the shoulder of the active element, by the depth of penetration of the active element in the joint structure and by the values of the technological parameters. The following are highlighted.

- The major impact on the values of the roughness is from the material positioned at the top of the welded structure, in direct contact with the shoulder of the active element: the smallest values of the roughness (max. 2,7 μm) were recorded at structure 1, at which the AA2024 alloy was positioned at the top of the welding seam, and the highest roughness values (max. 15 μm) were recorded at structure 3, where the AA7075 alloy was positioned at the top of the welding seam (Fig. 7.3.2, 7.3.4 and 7.3.6);
- The variation of the roughness values along the welding seam is different depending on the structure analyzed, respectively, on the material positioned at the top of the welding seam. Structures 1 showed a stable evolution along the welding seams for each experiment, respectively, Ra: 1,2 – 2,7 μm . Structures 2 showed a decreasing evolution of the roughness along the welding seam [B12], respectively, Ra: 10,5 – 0,8 μm , and structures 3 showed an increasing evolution with respect to the evolution of the welding seam, respectively, Ra: 0,9 – 14,7 μm (Fig. 7.3.2, 7.3.4 and 7.3.6);
- The analysis of the influence of the technological parameters n and w on the roughness of the welding seam was performed for the stabilized area of the process (zone/ sample 3), finding that they have a variable influence depending on the analyzed structure. At structure 1, the increase of the two technological parameters leads to the decrease of the roughness Ra in area 3. For structures 2 and 3, the evolution of the roughness Ra according to the technological parameters is not relevant, but having a tendency to decrease with the increase of the welding speed.

7.4. The macrostructure of welding seam

The macrostructure of the welded structure, an important feature of it, was analyzed as presented in sub-chapter 6.9, respectively, on two samples extracted from the welded structure, for each of the 18 preliminary experiences. Also, a visual analysis of the upper part of the joint was performed. Images of the macrostructure and the upper part of the joints are presented for structures 1, 2 and 3 is represented in Fig. 7.4.7, 7.4.9, 7.4.14 and 7.4.16.

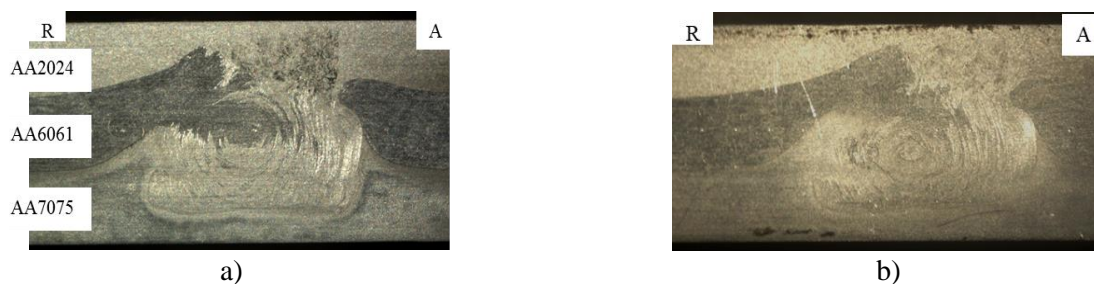


Fig. 7.4.7. Macrostructure and visual aspect of structure 1, exp. 1.6: a) sample 1.6.1; b) sample 1.6.2; A – advancing side; R – retracting side

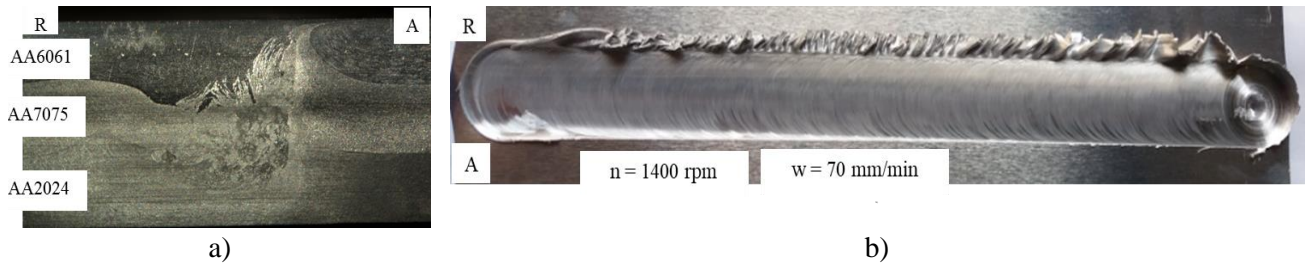


Fig. 7.4.9. Macrostructure and visual aspect of structure 2, exp. 2.2: a) sample 2.2.1; b) the upper side of the joint; A – advancing side; R – retracting side

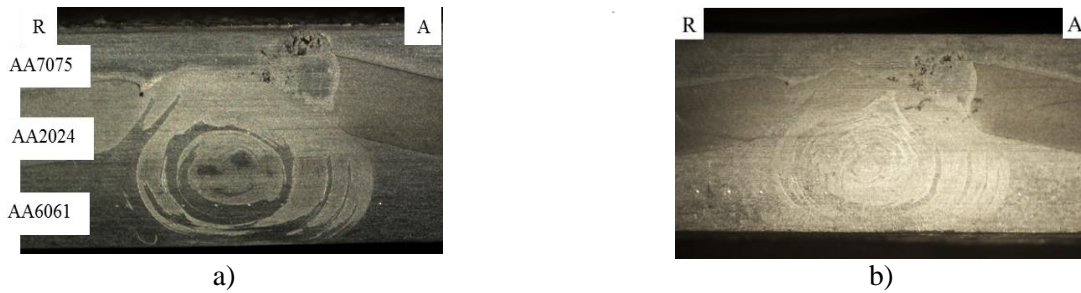


Fig. 7.4.14. Macrostructure and visual aspect of structure 3, exp. 3.1: a) sample 3.1.1; b) sample 3.1.2; A – advancing side; R – retracting side

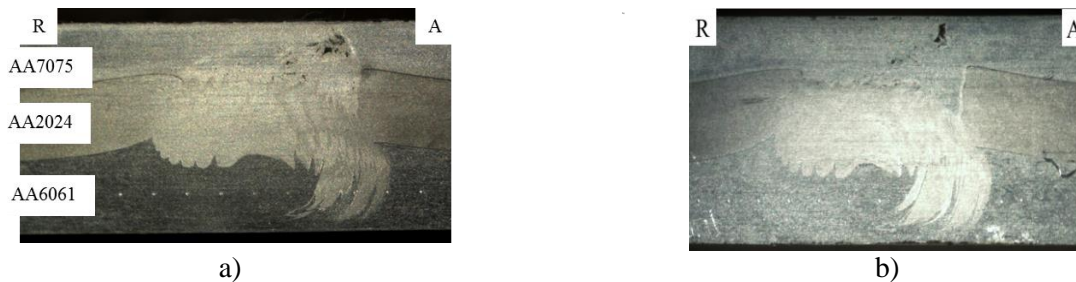


Fig. 7.4.16. Macrostructure and visual aspect of structure 3, exp. 3.3: a) sample 3.3.1; b) sample 3.3.2; A – advancing side; R – retracting side

The analysis of the macrostructure of welded structures 1, 2, 3 highlights the following.

- Structure 3 (AA7075 – AA2024 – AA6061) is the one with the least defects. This is due, on the one hand, to the positioning of the AA7075 and AA2024 alloys in contact, in the upper part, in the area where the active welding element penetrates completely and, on the other hand, the compatibility of the two materials [B10]. For the alloy positioned in the lower area, the rotating active element penetrates 70 - 80%, the amount of material displaced and mixed with the other two being smaller. Also, the positioning of the AA7075 alloy on the top has led to the avoidance of burr defects;
- The technological parameters influenced the macrostructural characteristics of the welded joints:
 - at structure 1, the best results are found in the area of average values of the two technological parameters, but the increase of the welding speed and the increase of the rotation speed negatively affect the macrostructural aspect of the welding seam;
 - at structure 2, the best results are found at the upper rotation speed limit and the lower welding speed limit; the largest number of experiences with faults was identified; one cause of the large number of defects may be the joining of the alloys AA6061 and AA7075 in the upper area of the structure;
 - at structure 3, the values of the parameters that led to the best results are the minimum value of the rotation speed; but the increase of rotation speed of active element negatively influences the macrostructural aspect of the welding seam [B11];

- All the experiences in which maximum values of the technological parameters were used simultaneously, $n = 1400$ rpm and $w = 170$ mm/min, have led to structures with major defects of channel type, crack etc.

7.5. The microstructure of the welding seam

The microstructure of the welding seam, an important feature of it, was analyzed as presented in sub-chapter 6.9, respectively, on a test piece from each welded structure, by selecting from the sample with the least macrostructural defects, based on the conclusions, shown in sub-chapter 7.4 (Fig. 7.5.4 and 7.5.5).

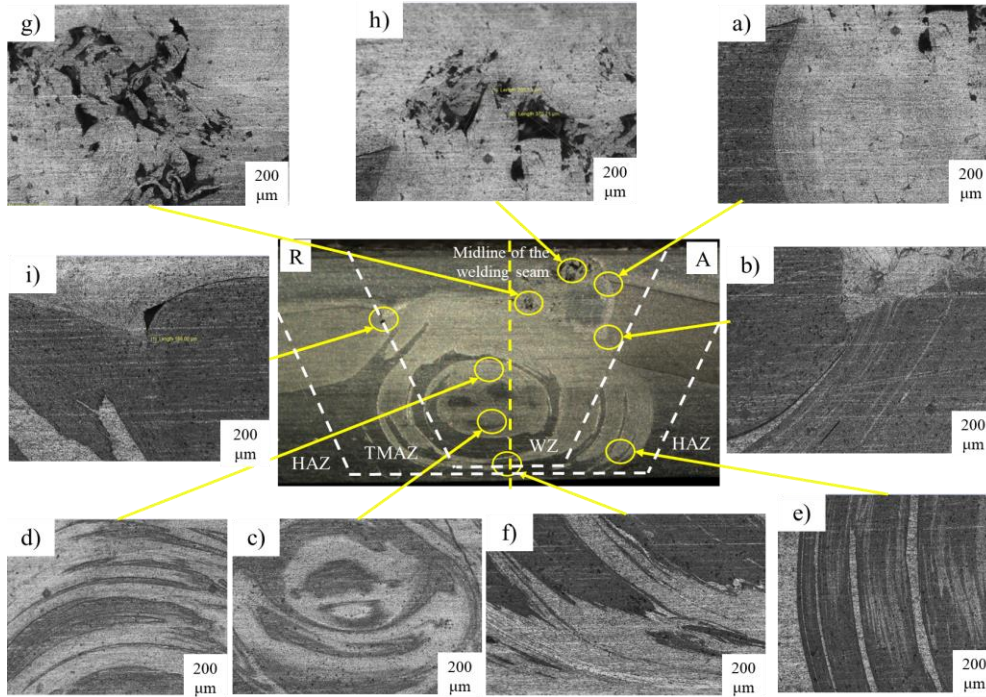


Fig. 7.5.4. Microstructure of sample 3.1.1 (structure 3/ AA7075 - AA2024 - AA6061): a), b), c) and d) creep in the welding zone; e) and f) creep in the thermally and mechanically affected zone; g), h) și i) defects in the welding zone; A – advancing side; R – retracting side

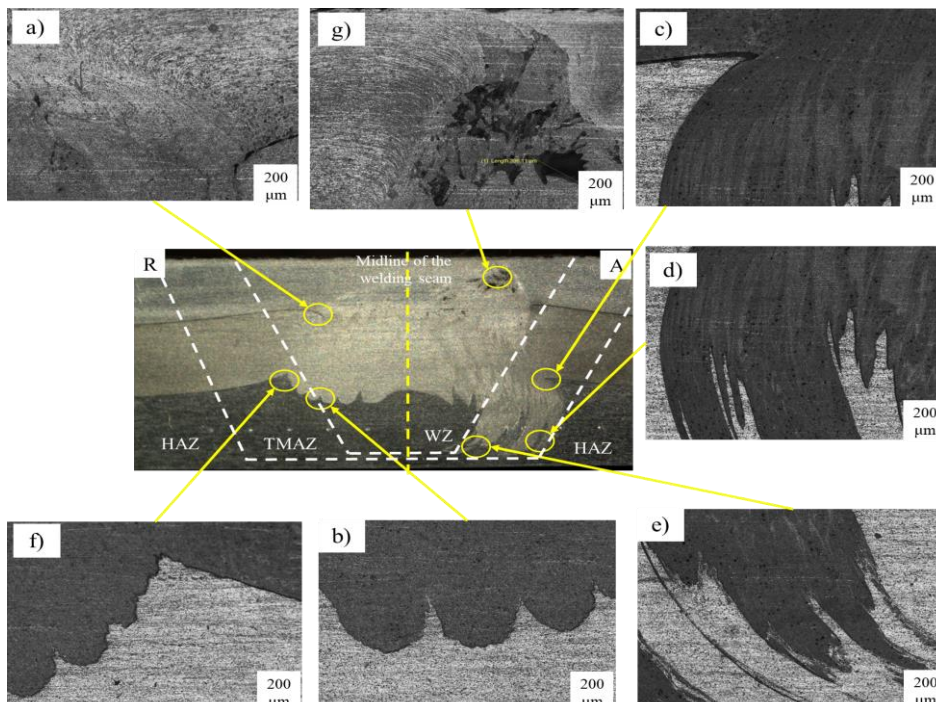


Fig. 7.5.5. Microstructure of sample 3.3.1 (structure 3/ AA7075 - AA2024 - AA6061): a) and b) creep in the welding zone; c), d), e) and f) creep in the thermally and mechanically affected zone; g) defects in the welding zone; A – advancing side; R – retracting side

From the analysis carried out in relation to the microstructure of welded joints, the following conclusions can be drawn:

- At structure 3, for n and w of minimum values (exp. 3.1), the maximum degree of mixing of the three alloys is achieved, a well-defined welding area, symmetrical on both the advance and the retracting side, with the lowest defect rate;
- All four samples analyzed have a well-marked creep between the three aluminum alloys, identifying the boundary between materials, which confirms the impossibility of mixing them at the molecular level, due to insufficiently high temperatures during the process;
- The position of the defects varies in the welding seam depending on the joint structure, respectively, the position of the welding materials within it; if the AA2024 alloy is positioned at the bottom, the defects appear predominantly in the lower area, and when this alloy occupies the upper or middle position, the defects appear in the upper area of the welding seam.

7.6. The microhardness of the welding seam

The microhardness of the welding seam, an important feature of it, was analyzed as presented in sub-chapter 6.10, respectively, on two samples from each welded structure/ experience – to highlight the evolution of the microhardness along the welding seam. In the same working conditions, for comparative analysis, the microhardness was measured also in areas adjacent to the welding seam, as well as the basic materials.

Table 7.6.1. Average values of the microhardness of the basic materials

Base material	Average of microhardness [HV 0.3]
AA2024	141,3
AA6061	41,1
AA7075	188,8

It is mentioned that in the areas with defective joints, no microhardness measurements were made.

The microhardness of base materials – AA2024, AA6061 and AA7075 – is presented in Table 7.6.1. The microhardness of the basic materials and the evolution of the microhardness of the area comprising the welding seam are presented in Fig. 7.6.8, 7.6.10, 7.6.14 and 7.6.16.

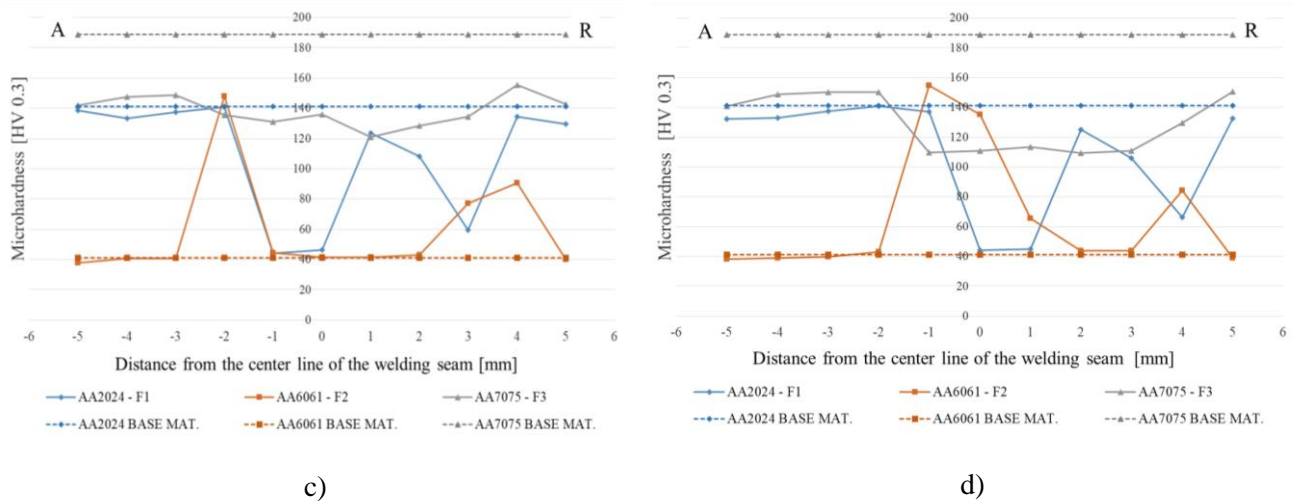


Fig. 7.6.8. Variation of microhardness in: c) sample 1.6.1; d) sample 1.6.2;

A – advancing side; R – retracting side

(exp. 1.5 and 1.6: n = 1000 rpm, w = 120 mm/min, structure 1/ AA2024 – AA6061 – AA7075)

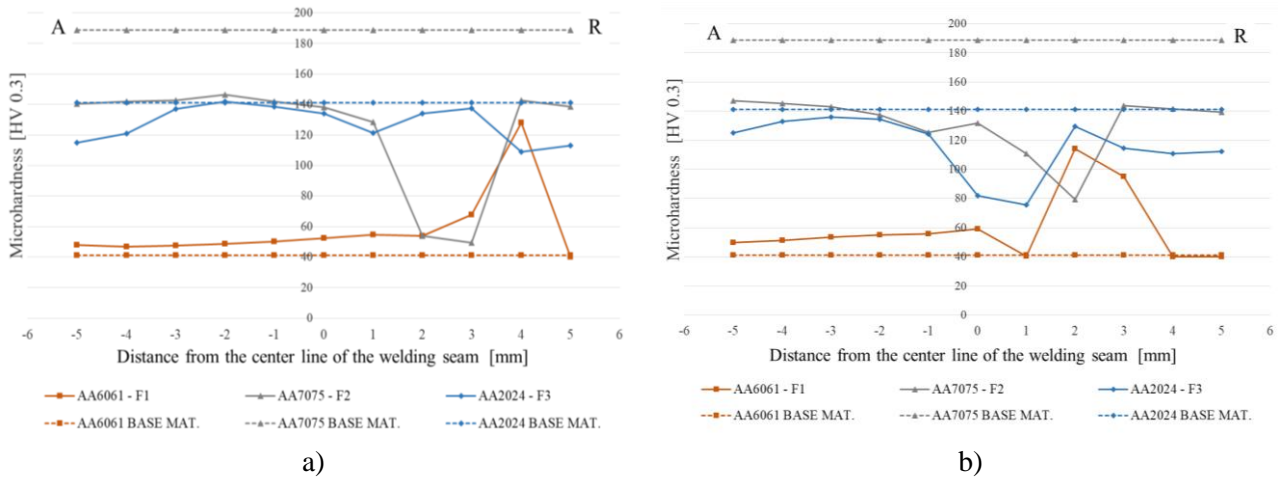


Fig. 7.6.10. Variation of microhardness in: a) sample 2.2.1; b) sample 2.2.2; A – advancing side; R – retracting side (exp. 2.2: n = 1400 rpm, w = 70 mm/min, structure 2/ AA6061 – AA7075 – AA2024)

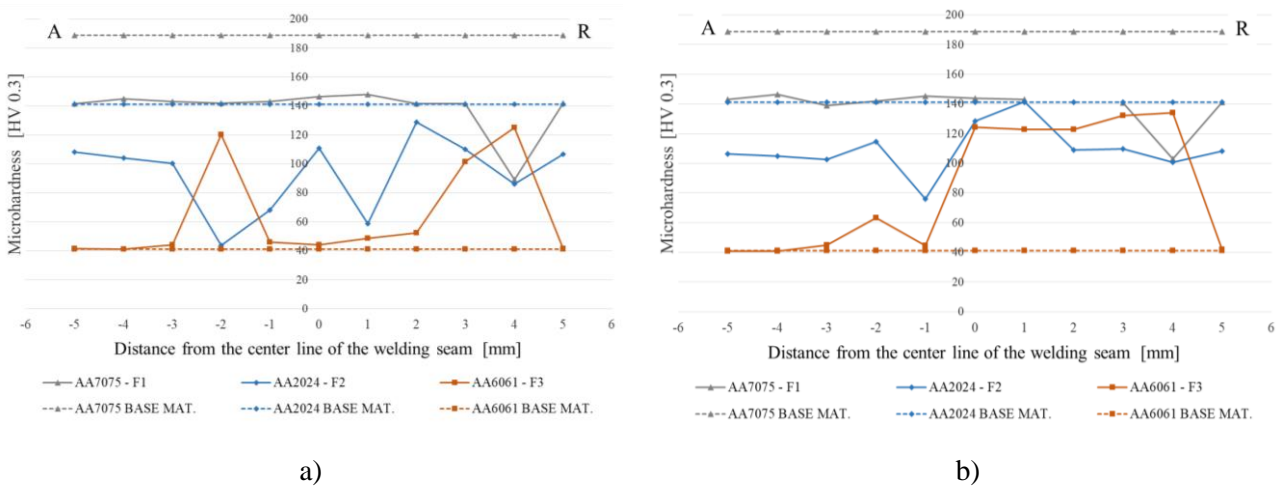


Fig. 7.6.14. Variation of microhardness in: a) sample 3.1.1; b) sample 3.1.2; A – advancing side; R – retracting side (exp. 3.1: n = 600 rpm, w = 70 mm/min, structure 3/ AA7075 - AA2024 - AA6061)

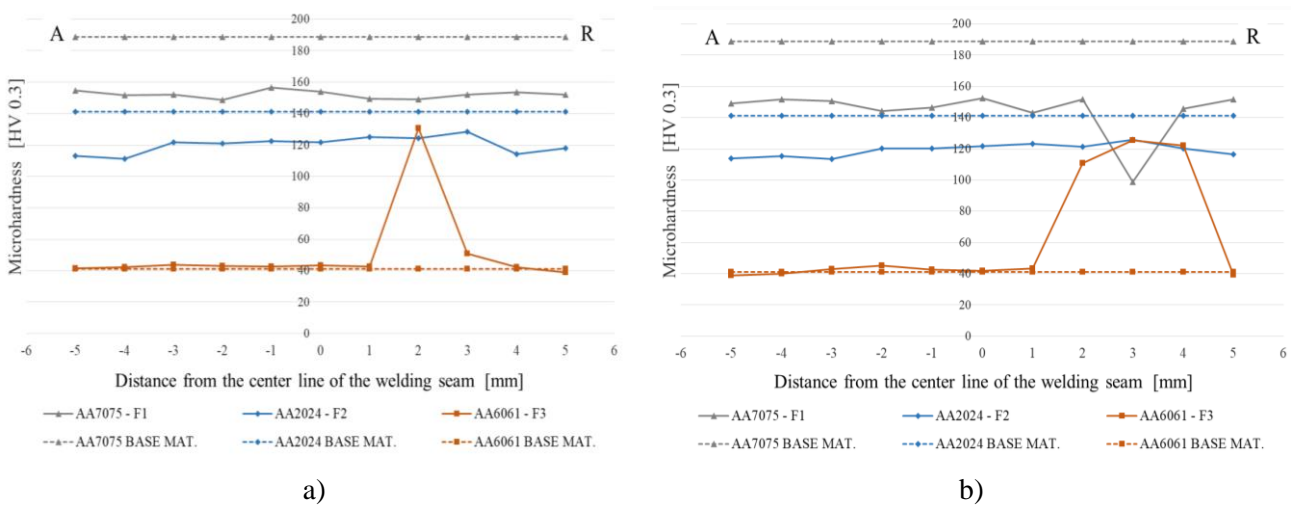


Fig. 7.6.16. Variation of microhardness in: a) sample 3.3.1; b) sample 3.3.2; A – advancing side; R – retracting side (exp. 3.3: n = 600 rpm, w = 170 mm/min, structure 3/ AA7075 – AA2024 – AA6061)

The average values of the microhardnesses of the welded structures analyzed are as shown in Table 7.6.2.

Table 7.6.2. The average values of the microhardnesses of the welded structures analyzed

Material/ Filiation	Average values of microhardness [HV 0.3]			
	Base material	Structure 1 (AA2024 – AA6061 – A7075)	Structure 2 (AA6061– AA7075 – AA2024)	Structure 3 (AA7075 – AA2024 – A6061)
AA2024	141,3	102,6	115,9	100
AA6061	41,1	77,5	72,2	87
AA7075	188,8	132	106,6	125,3

The highest homogeneity of the values of microhardness is found in structure 3, which can be explained by the fact that it has the best mixing degree of the three materials and the smallest number of defects [B10].

Chapter 8. Results of the advanced theoretical - experimental research on the friction stir welding process and system of different aluminum alloys structures

Results of the advanced theoretical – experimental research and numerical modeling regarding the friction stir welding of structures of different aluminum alloys, which also include published elements of the author [C17, G06], are presented below, grouped on the sizes analyzed during research.

8.1. Advanced experimental program

Advanced theoretical – experimental research is based on the methodological reference elements and the experimental research system, as well as elements derived from conducting and analyzing the main results of preliminary theoretical – experimental research (s. chapters 5, 6, 7).

Welding structure

Considering the conclusions drawn from the preliminary theoretical – experimental researches, according to which structure 3 (AA7075 – AA2024 – AA6061) presents the best degree of material mixing, with favorable effects on the properties of the structure, the advanced theoretical – experimental researches were realized on a single structure, namely structure 4/ AA7075 – AA2024 – AA6061 (Table 5.3.4), in which the component plates/ parts are totally superimposed, compared to structure 3, whose parts/ component plates – of the same materials and with the same positioning – are partially superimposed.

The characteristics of the welding process are the process temperature and the axial process force.

The characteristics of the welded structure that are analyzed are: roughness, macrostructure, microstructure, microdrenth, tensile strength and relative elongation.

8.2. Process temperature and axial process force

Based on the characteristics of the process temperature evolutions, it is possible to determine the average process temperature in the welding zone/ phase, T_{med} (v. § 7.1), which is presented in Table 8.2.1 and Fig. 8.2.6.

Based on the characteristics of the evolution of the axial process force, the sizes can be associated $F_{a\ max-p}$, $F_{a\ max-s}$, $F_{a\ med-s}$, d_s (s. § 7.2), which are presented in Table 8.2.1 and Fig. 8.2.7 – 8.2.10.

Table 8.2.1. Values of the specific quantities associated with the process temperature in the welding zone / phase and the axial process force

Exp. code	Technological parameters		T_{med} [°C]	$F_{a\ max-p}$ [kN]	$F_{a\ max-s}$ [kN]	$F_{a\ med-s}$ [kN]	d_s [mm]
	n [rpm]	w [mm/min]					
4.1	650	60	460	11,8	11,6	11	43
4.2	1100	60	490	8,9	9,5	8,9	93
4.3	650	100	470	12,3	12,4	12	36
4.4	1100	100	505	10	9,7	9	36
4.5	845	80	475	10,7	12	11,5	48
4.6	845	80	480	10,5	12,2	11,9	55

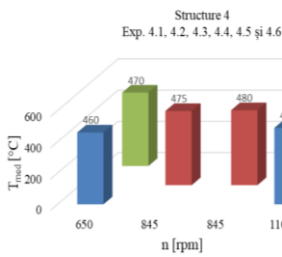


Fig. 8.2.6. The average process temperature in the welding zone/ phase, T_{med} , depending on n and w

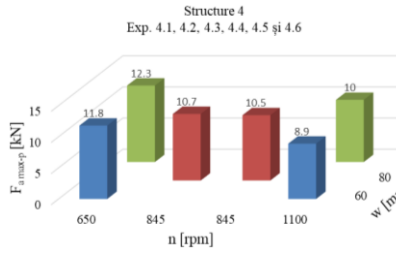


Fig. 8.2.7. The maximum value of the axial force characteristic of the penetration phase, $F_{a\ max-p}$, depending on n and w

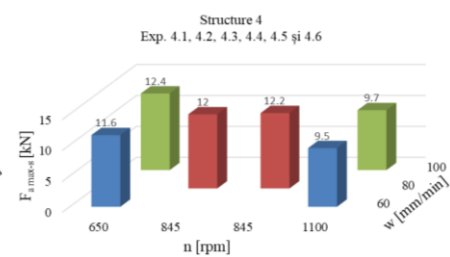


Fig. 8.2.8. Fig. 7.2.7. The maximum value of the axial force characteristic of the welding phase, $F_{a\ max-s}$, depending on n and w

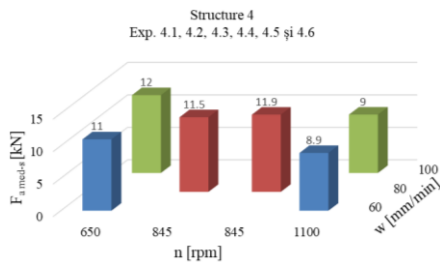


Fig. 8.2.9. The average value of the axial force characteristic of the stabilized welding area, $F_{a\ med-s}$, depending on n and w

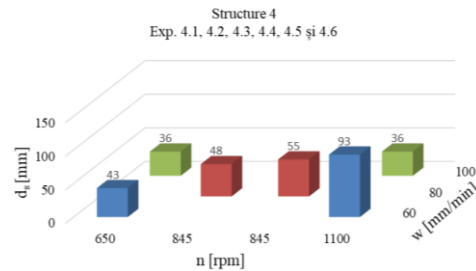


Fig. 8.2.10. The longitudinal distance until the axial force/ process stabilization, d_s , in according to n and w

Data analysis highlights a series of dependencies. The following are highlighted.

- Increasing the rotation speed of the rotating active element leads to the increase of the temperature during the process and, implicitly, to the decrease of the axial process force (Table 8.2.1 and Fig. 8.2.6 – 8.2.9);
- The welding speed directly influences the process temperature to a lesser extent than the rotation speed (Table 8.2.1 and Fig. 8.2.6). Also, the increase of the welding speed leads to the increase of the axial process force (Table 8.2.1 and Fig. 8.2.7 – 8.2.9). The highest value of the axial force during the process was reached at exp. 4.3, whose technological parameters were: the minimum value of the rotation speed and the maximum value of the welding speed;
- The technological parameter with the highest weight on the output parameters is the rotation speed: at an increase of 70 % of the rotation speed, the temperature during the process increased by about 7 %, and the axial maximum process force decreases by 22 %;
- The stabilization distance of the process, d_s , is dependent on: the parameters n and w, as well as the period of maintenance of the rotating active element in the material penetration phase. For structure 4, d_s increases with increasing rotation speed and decreases with increasing welding speed (Fig. 8.2.10 and Table. 8.2.1). It is assumed that the longer the holding period of the rotating active element at the end of the penetration phase without advancing speed, the shorter the stabilization distance of the process, because a faster temperature rise occurs before the beginning of the zone/ welding phase.

8.3. The roughness of the welding seam

The roughness of the welding seam was measured in three specific areas for each welding seam for all six experiences (v. § 6.8). The dependence of the average value of the roughness Ra on the position of the specimen within the structure is shown in Fig. 8.3.2.

The following conclusions are drawn:

- increasing the rotation speed of the rotating active element and decreasing the welding speed lead to a slight decrease in the roughness: difference between the maximum value and the minimum value of the roughness in area 3 is 1,8 μm ;
- the evolution of the roughness values along the welding seam has the tendency to stabilize along the joint, with decreasing tendency for most experiences – 4.2, 4.4, 4.5 and 4.6 (Fig. 8.3.2). For all welding seam made with different technological parameters, the overall average roughness value is about 8,5 μm .

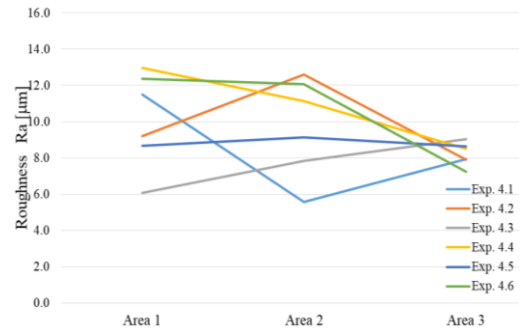


Fig. 8.3.2. Average values of roughness at structure 4

8.4. The macrostructure of welding seam

The macrostructure of the welding seam was analyzed in two areas of each welding seam (§ 6.9), with the mention that the specimens in the welded structure at exp. 4.3 are shifted by 40 mm to the starting area of the joint, because the rotating active element failed during the process (Fig. 8.4.4).

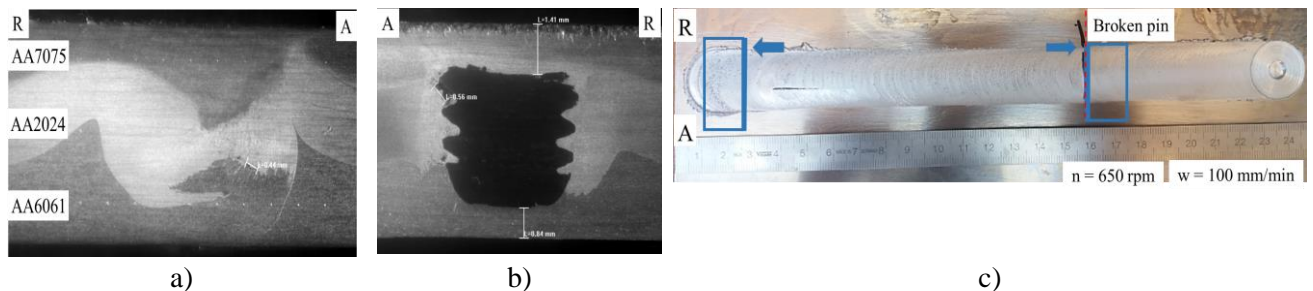
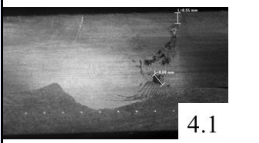
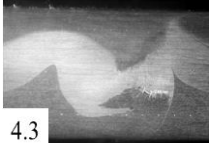
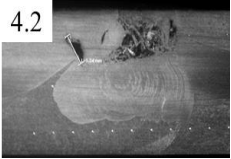
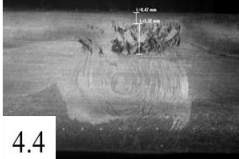


Fig. 8.4.4. Macrostructure and visual aspect of structure 3, exp. 4.3: a) sample 4.3.1; b) sample 4.3.2; c) the upper side of the joint; A – advancing side; R – retracting side

The analysis of the microstructure of the joint 4 highlights the following.

- Burr defects are absent from these experiments, which is due to the positioning in the upper part of the structure of the material AA7075 (the material with higher hardness), in direct contact with the tool shoulder;
- Increasing the welding speed decreases the rate of occurrence of defects in the welding seam section. Comparing the macrostructure of the joints obtained with the experiments performed with the welding speed of 60 mm/min with the macrostructure of the joints obtained in the experiments performed with 100 mm/min, we can observe an improvement of the macrostructural aspect and a decrease of the defects (Table 8.4.1);
- Increasing the rotation speed improves the shape and appearance of the welding area, but at the same time leads to the appearance of defects, in the upper area of the joint. Experiments with a rotation speed of 650 rpm lead to the lowest defect weight in the welding seam (Fig. 8.4.4), and experiences with a speed of 1100 rpm lead to the highest defect in the welding seam (Table 8.4.1).

Table. 8.4.1. Centralization of macroscopic images related to the rotation speed and welding speed values

		The welding speed [mm/min]		
		60	80	100
The rotation speed [rpm]	650	 4.1	-	 4.3
	845	-	 4.5  4.6	-
	1100	 4.2	-	 4.4

From the above, it turns out that the best macrostructure of the joints is obtained for the use of the technological parameters n and w with values of 600 – 650 rpm and, respectively, 70 – 100 mm/min.

8.5. The microstructure of the welding seam

The microstructure of the joint 4 was analyzed in the specimen with the least macrostructural defects, respectively, the specimen 4.3.1 – related exp. 4.3/ $n = 650$ rpm and $w = 100$ mm/min, based on the conclusions drawn from sub-chapters 7.5 and 8.4. Characteristic elements of the microstructure of specimen 4.3.1 (Fig. 8.5.2) are the following.

- The degree of mixing of the three materials in the welding area is at an average level, it falls between the one obtained at the exp. 3.3 (Fig. 7.5.5), $n = 600$ rpm and $w = 170$ mm/min, and that obtained at exp. 3.1 (Fig. 7.5.4), $n = 600$ rpm and $w = 70$ mm/min. It can be concluded that decreasing the welding speed, up to a certain value, improves the mixing degree of the materials in the welding area of the joints, after which it can facilitate the appearance of defects (Table 8.4.1);
- The creep between the three alloys is well realized, but the boundaries between the different materials are highlighted. Similar to structures 1, 2, 3, analyzed previously (s. sub-chapter 7.5), it is confirmed that they cannot be mixed at the molecular level (Fig. 8.5.2: a, b, c, d, e, f and g). The heat generated by the friction determines the softening of the materials and thus their creep, but the temperature of the process is not high enough to lead to the formation of new phases, without reaching the melting points of the alloys used;
- In the welding zone (WZ) the grains are fine and equiaxial, due to the recrystallization annealing determined by the temperature at which the material reaches by rotating the rotating active element and the high degree of plastic deformation (Fig. 8.5.2: a and b). In the thermo-mechanically influenced zone (TMAZ), the temperature is not strong enough to produce recrystallization (Fig. 8.5.2: c and d), this area being characterized by strongly deformed grains. In the thermally influenced zone (HAZ), there are no mechanical changes;
- The area of defect occurrence is positioned on the feed side, at the boundary between the middle material (AA2024) and the material positioned at the bottom (AA6061). Similar to structures 1, 2, 3 (s. sub-chapter 7.5), an area of defects mainly on the forward part of the rotating active element is observed. The distribution of defects on the feed side can be caused by the pin shape of the rotating active element – cylindrical M6 (Fig. 8.5.2: h; Fig. 7.5.5: g; Fig. 7.5.4: g, h and i) and the sense rotational movement of the active rotating welding element; by this combination, move the material from the lower area to the upper zone and from the advance area (A) of the rotating active element to the retracting area (R);

- The size of the largest pore identified is about 216,5 μm, being smaller than the pores identified in the other experiences, for both structure 4 and structure 3.

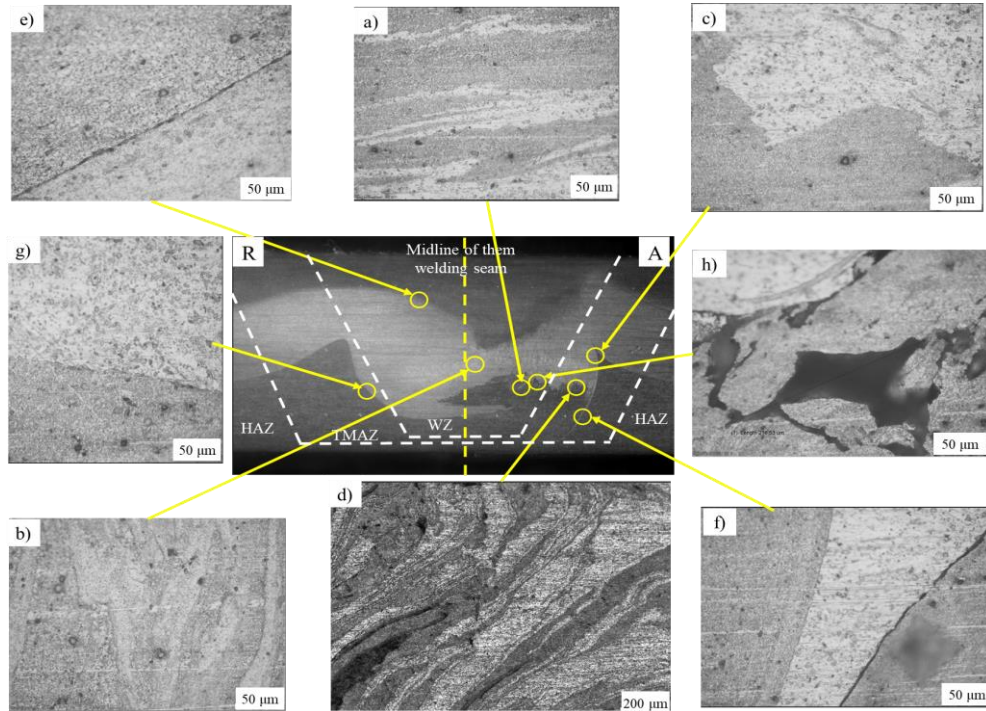


Fig. 8.5.2. Microstructure of sample 4.3.1 (structure 4/ AA7075 – AA2024 – AA6061): a) and b) creep in the welding zone; c) and d) creep in the thermally and mechanically affected zone; e), f) and g) the boundaries between the materials; h) defects in the welding zone; A – advancing side; R – retracting side

8.6. The microhardness of the welding seam

The microhardness of the welding seam was analyzed in two areas of each welding seam (§ 7.6), respectively, to the two sample from each of the six advanced experiences – to highlight the evolution of the microhardness along the joint, noting that the specimens in the welded structure at exp. 4.3 are offset by 40 mm to the starting area (s. sub-chapter 8.4).

The microhardness of the basic materials and the evolution of the microhardness of the area comprising the welding seam are in Fig. 8.6.4, with the indication that the microdurity values of the basic materials are those set in sub-chapter 7.6

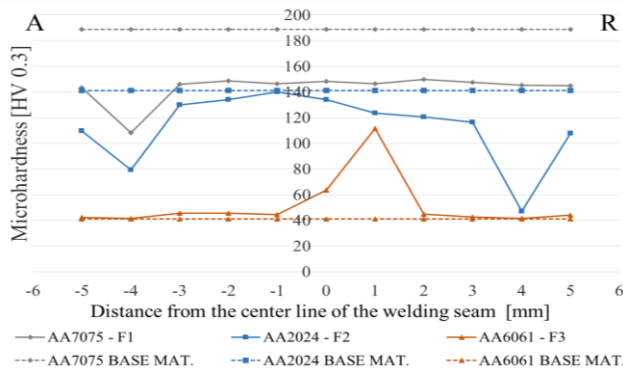


Fig. 8.6.4. Variation of microhardness in: sample 4.3.1; A – advancing side; R – retracting side (exp. 4.3: n = 650 rpm, w = 100 mm/min, structure 4/ AA7075 – AA2024 – AA6061)

The analysis of the data regarding the microhardness of structure 4 highlights the following.

- The microhardness filiations (F1, F2, F3) were completed in sample 4.3.1 (Fig. 8.6.4), which showed a higher degree of mixing of the three materials and a small number of defects, in the rotation speed conditions of the minimum value and the maximum value of welding speed (exp. 4.3/ n = 650 rpm, w = 100 mm/min);

- The microhardness is stabilized along the welding seam, with the removal of the rotating active element from the beginning of the joint, following the improvement of the mixing degree of the materials and the decrease of the number of defects in the seam (the samples x.x.2, each experience);
- The values of the microhardness of the filiation made on the material positioned at the top of the joint (AA7075) are about 21 % lower than the values of microhardness of the basic material AA7075. This decrease is due, in particular, to the high temperature recorded in this area of the structure during the process and less to the mechanical mixing of the three materials, an aspect demonstrated by the differences recorded in the HAZ area of the welding seam (positioned at 5 – 6 mm from the the median plane of the joint) (Table 8.6.1);
- The values of the microhardness of the filiation made on the material positioned in the middle of the structure (alloy AA2024) are lower by about 16 % than those of the basic material AA2024. This decrease is also due to the temperature increase during the process in the HAZ area and the mechanical mixing of the three alloys (Table 8.6.1);
- The values of the microhardness of the filiation made on the material positioned at the bottom of the structure (alloy AA6061) are about 19 % higher than those of the basic material AA6061, being the only filiation that increased after the FSW welding process. This increase is due, in particular, to the mechanical mixing of the three materials and to a lower temperature in this area during the process (Table 8.6.1).

Table 8.6.1. Average values of microhardness depending on rotation speed and welding speed

Exp. code	Technological parameters		T_{med} [°C]	Filiation F1 (AA7075)	Filiation F2 (AA2024)	Filiation F3 (AA6061)
	n [rpm]	w [mm/min]				
4.1	650	60	460	145,4	115,2	42,1
4.2	1100	60	490	150,6	119,7	59,5
4.3	650	100	470	143,3	113	51,7
4.4	1100	100	505	150,8	125,3	43,6
4.5	845	80	475	150,1	124,1	53,6
4.6	845	80	480	149,3	113,6	42,6
Average values of micro-hardness for all experiences				148,2	118,5	48,8
Basic material micro-hardness				188,8	141,3	41,1
The average percentage variation of the microhardness of the welded structure versus the microhardness of the base material				- 21 %	- 16 %	+ 19 %

8.7. The tensile strength of the welded structure

The tensile strength of the welded structure on specific sample, taken from welded structures or basic materials, shall be carried out on the basis of elements covered by the standard SR EN ISO 6892-1:2010 [S18] or/and presented in the expert treaties/ published scientific papers [R08].

Thus, in order to characterize the behaviour of specific sample during the tensile test, the following sizes shall be considered, as appropriate:

- the area of the initial cross-section, S_0 , and the initial length between two points associated with the calibrated part of the sample, L_0 or l_0 ;
- time, t , as duration;
- tensile force, F , as well as maximum force, F_m , respectively, the maximum tensile force value (the highest force borne by the sample during the tensile test);
- the length of the calibrated area of the test tube on which the elongation is measured at any time, L or l , as well as the elongation (extension) of the sample, or ΔL , respectively, Δl ;
- the base length of the extensometer, L_e , as well as the elongation or extension at breakage, ΔL_f .

On the basis of the above elements and definition expressions, the dependency relationships and specific sizes shall be determined as follows:

- variation of tensile force, F , over time, t , as well as maximum force, F_m , $F = f(t), t \in D_t$ (8.7.1)

respectively, $F_m = \max f(t), t \in D_t$ (8.7.2)

- elongation of the sample, ΔL or Δl , respectively: $\Delta L = L - L_0, \Delta l = l - l_0$ [mm] (8.7.3)

- conventional tension, σ , and conventional relative elongation, ε , $\sigma = \frac{F}{S_0}$ [MPa], $\varepsilon = \frac{\Delta L}{L_0}$ sau $\varepsilon = \frac{\Delta l}{l_0}$ (8.7.4)

- actual tension, σ_v , and actual relative elongation, ε_v , $\sigma_v = \sigma(1 + \varepsilon), \varepsilon_v = \ln(1 + \varepsilon)$ (8.7.5)

- tension, σ , depending on the relative elongation, ε , $\sigma = \varphi(\varepsilon), \varepsilon \in D$ (8.7.6)

- actual tension, σ_v , depending on the actual relative elongation, ε_v , respectively: $\sigma_v = \varphi_v(\varepsilon_v), \varepsilon_v \in D_v$ (8.7.7)

- tensile strength, R_m , as the tension corresponding to the maximum force, F_m , respectively: $R_m = \frac{F_m}{S_0}$ [MPa] (8.7.8)

- elongation/ total percentage extension at breaking, A , which, in order to simplify expression, will continue to be called the relative elongation at breakage, respectively: $A_t = \frac{\Delta L_f}{L_e} 100$ [%] (8.7.9)

To highlight that, in general, the relationship f , the relationship φ , the scope of work/ definition D_t , etc. depend on a number of factors, including the structural and connecting characteristics of the weld seam - sample are determining.

Next, in order to highlight the characteristics associated with the welded structures studied, corresponding to each group of four test tubes in the structure welded to an experience: dependence tensile force – time, $F - t$ (rel. 8.7.1), on the same graph, the maximum forces F_m (rel. 8.7.2) – on the same graph, the position of the test tubes within the welded structure and images captured during the tensile test, respectively, which highlight the sensitive areas of the joint that caused it to break, in order to break the three materials/ plates of the welded structure [C17, G06].

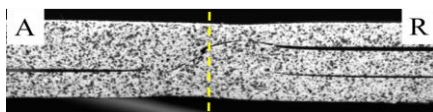


Fig. 8.7.14. Breakage in sample 4.3.4 - in the porous defect for AA2024

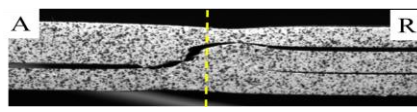


Fig. 8.7.15. Breaking the sample 4.3.4 – AA2024

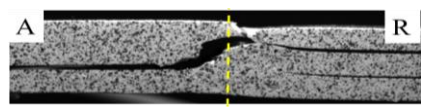


Fig. 8.7.16. Breaking the sample 4.3.4 – AA7075

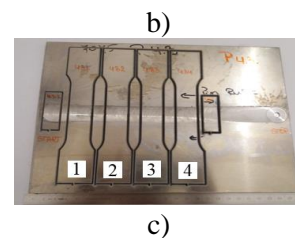
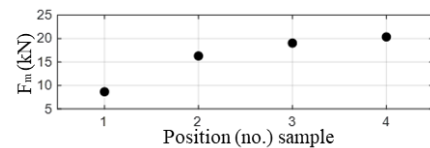
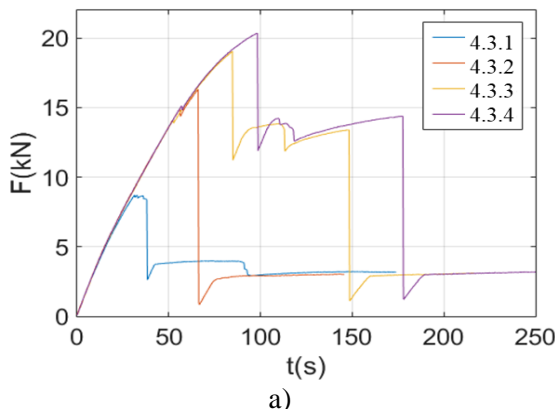


Fig. 8.7.13. Tensile test of samples 4.3.1 – 4.3.4: a) dependence $F - t$; b) maxim force F_m ; c) position of the samples (structure 4/ AA7075 – AA2024 – AA6061, exp. 4.3/ $n = 650$ rpm, $w = 100$ mm/min)

From the analysis of the above data, the following are shown.

- In all the tests performed, the joint failed from the defective area (tunnel, pores, non-homogeneous core) of the welding seam, regardless of their position – advancing side or retracting side of the rotating active element (Fig.8.7.14 – 8.7.16) [G06]. Because these defects are predominantly located in the area of the material positioned on the upper part of the structure, AA7075 (with the smallest A_t), the breakdown of the structure started from the area of this material. The breakdown of the structure continued with the breakdown of the material positioned in the middle of the structure, AA2024 (with the medium value of A_t). The last material in the structure that failed during the tensile test was the one positioned at the bottom, AA6061 (with the maxim value of A_t);
- The evolution of the maximum breaking force, F_m , of the samples in the specific area of the welding seam is not similar for all the experiments performed: a decreasing evolution of this force along the welding seam was observed in experiments 4.1, 4.2 and 4.4 and an increasing evolution at experiences 4.3, 4.5 and 4.6 (Fig. 8.7.13). The experiences for which the F_m evolution along the welding seam was decreasing are those experiences with the highest number of defects in the welding seam section. These experiments were performed at least with the rotation speed at the maximum value (1000 rpm) or the welding speed at the minimum value (60 mm/min) [C17, G06].

The dependencies average F_m – n or/and w, average R_m – n or/and w, and average A_t average – n or/and w are presented in Fig. 8.7.27, 8.7.28, respectively, 8.7.29:

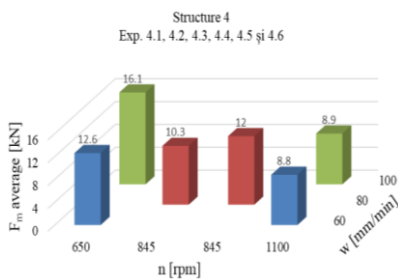


Fig. 8.7.27. The average maximum force, F_m average, based on n and w

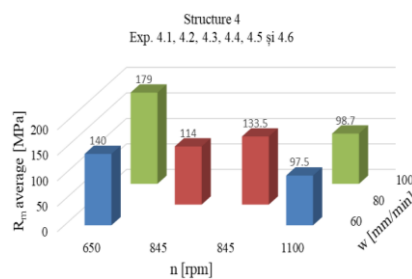


Fig. 8.7.28. The average tensile strength, R_m average, based on n and w

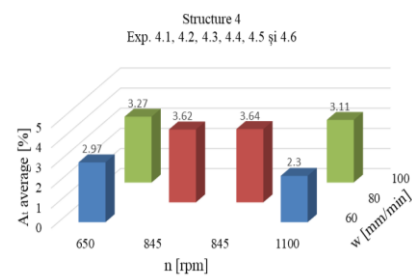


Fig. 8.7.29. The average relative elongation, A_t average, based on n and w

Highlight the following.

- Increasing the rotation speed n leads to the decrease of all these parameters F_m , R_m and A_t , respectively (Fig. 8.7.27 – Fig. 8.7.29): in the experiences with the lowest value of the rotation speed (650 rpm) the highest values were recorded (Fig. 8.7.13), and in the experiences with the highest value of the rotation speed (1100 rpm) the lowest values were recorded;
- The increase of the welding speed w leads to the increase of all these parameters F_m , R_m și A_t , respectively (Fig. 8.7.27 – Fig. 8.7.29) [C17]: at the experiences with the lowest value of the welding speed (60 mm/min) were recorded lower values, and at the experiences with the highest value of the welding speed (100 mm/min) higher values were recorded (Fig. 8.7.13);
- The specimens with the best characteristics F_m , R_m și A_t , identified by the tensile test, are the specimens associated with exp. 4.3/ minimum rotation speed and maximum welding speed (n = 650 rpm, w = 100 mm/min); the properties improve along the welding seam (from beginning to end) [G06] which is consistent with the results of the macroscopic analysis, which revealed the existence of the best macrostructural aspect and a minimum number of defects (Fig. 8.4.4).

8.8. Case study on analysis of structures by tensile strength test and digital image correlation

Analysis of structures welded by tensile test and DIC (Digital Image Correlation) allows to determine the characteristics of the welded structures associated with the tensile test presented in § 8.7, as well as the determination of characteristics of the type of dependence mean real tension – real mean relative elongation, field of deformations, highlighting the action of inner defects, etc.

Thus, on the basis of the data during the tensile test of the sample 4.3.4 (Fig. 8.7.13), dependences of the actual mean tension type - actual mean relative elongation, $\bar{\sigma}_v - \bar{\epsilon}_v$, respectively,

$$\bar{\sigma}_v = f_v(\bar{\epsilon}_v) \tag{8.8.1}$$

Next, for the purpose of determining deformation field characteristics, the tensile force dependence – time, $F - t$, associated with the sample 4.3.4, $t = 0 - 50$ s (rel. 8.8.2 and Fig. 8.8.2), respectively,

$$F = f(t)_{4.3.4}, t \in [0; 50] \tag{8.8.2}$$

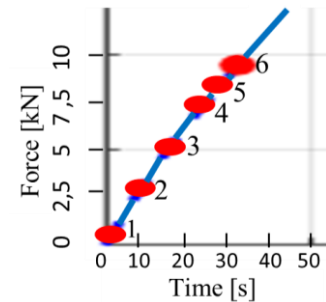


Fig. 8.8.2. Tensile force dependence – time, $F - t$, on tsample 4.3.4; states (F_i, t_i) : 1, 2, ..., 6

Dependence (rel. 8.8.3) determined on the basis of data from the tensil test of the 4.3.4 sample is shown graphically in Fig. 8.8.2 (Fig. 8.7.13, a).

In addition, a number of working values of the tensil force F, F_i , during the tensile test, as well as the corresponding states (F_i, t_i) , respectively:

$$F \in \{ F_i \mid i = \overline{1, 6} \},$$

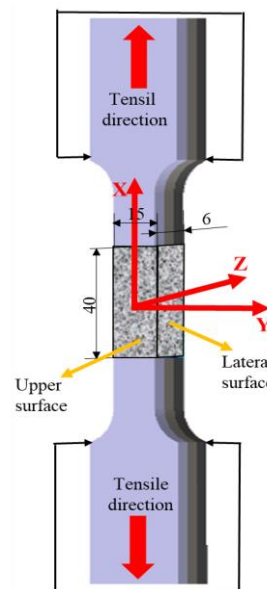
$$F_1 = 1 \text{ kN}, F_2 = 2,5 \text{ kN}, F_3 = 5 \text{ kN}, \tag{8.8.3}$$

$$F_4 = 7,5 \text{ kN}, F_5 = 8,5 \text{ kN}, F_6 = 10 \text{ kN}$$

$$(F_i, t_i) \in f(t)_{4.3.4}, i = 1, 2, \dots, 6 \tag{8.8.4}$$

as shown in Fig. 8.8.2.

Based on data processing through DIC (Digital Image Correlation), according to rel. 8.8.1 – 8.8.4, the deformation fields (relative elongations) for areas defined as part/ upper surface and side area/ lateral surface of the weld seam/ sample 4.3.4, as shown in Fig. 8.8.3 and Table 8.8.1 [C17, G06], were determined.



- Parts of the weld seam/ sample analysed
- Reference system: XYZ
- Area sizes with points – freckles:
 $l_0 = 40 \text{ mm}$,
 $b = 15 \text{ mm}$,
 $e = 6 \text{ mm}$.

Fig. 8.8.3. Reference elements for the definition of deformation fields (relative elongations)

Tabel 8.8.1. Deformation fields (relative elongations), ϵ_{xx} and ϵ_{xz} , in sample 4.3.4

i	F_i [kN]	The upper side/ surface of the welding seam		The lateral side/ surface of the welding seam		
		ϵ_{xx}		ϵ_{xx}		ϵ_{xz}
		0 0.5 1 1.5		0 0.5 1 1.5		-0.01 0 0.01
1	1					
6	10					

The analysis of these deformation fields highlights the following:

- The deformation fields recorded on the top of the welding seam attest that the maximum tensile values are located at the end of the welding zone, the TMAZ area and the HAZ area, arranged both on the advance side of the rotating active element and on the retracting part of the core; these deformation fields are also arranged longitudinally along the welding seam;
- From the point of view of the position of the deformation fields within the thickness of the welded structure, the most intense deformations are identified in the area of the median plane of the joint, respectively, between the median positioned material, AA2024, and the material positioned at the bottom of the structure, AA6061, on the advance side of the rotating active element (Fig. 8.5.2).

In relation to the above, it is stressed the usefulness of integrating, in tensile tests, the method DIC (Digital Image Correlation).

Chapter 9. Numerical modeling of the friction stir welding process of different aluminum alloy structures

Results of the numerical modeling regarding the friction stir welding process of different aluminum alloy structures, which also include published elements of the author [B07], are presented in the following.

9.1. Building the numerical model

The numerical model for the simulation of the FSW process of three different aluminum alloys was made for structure 4/ AA7075 – AA2024 – AA6061 (s. § 5.3.2 and chapter 8) and was constructed using the CEL (Coupled Eulerian-Lagrangian) technique, the software ABAQUS 6.13/ Explicit (s. § 5.3.3) [B07].

In the development of the numerical model, the following steps were taken: definition of the geometry of the welding structure and of the active rotating welding element; definition of the behavior of the three materials of the welding structure, by a law of behavior; definition of elastic and physical properties, as well as of heat transfer; defining the type of contact between the surfaces of the elements of the working system and the friction law; establishing the boundary conditions and process parameters; model discretization.

9.2. Validation of the numerical model

The numerical model validation was performed by comparing the simulated results with the results recorded during the process, under similar conditions, using two different techniques, which are based on comparing temperatures (v. § 3.8.1) and, respectively, comparing the appearance of the welding seam (s. § 3.8.4).

Validation of the numerical model using the temperature distribution in the welding seam

When validating the numerical model, with the help of temperature distribution in the welding seam, respectively, by comparing the temperatures achieved in the simulation with those recorded during the process, the following elements were considered:

- during the welding process, the temperature was measured with an infrared thermographic chamber (s. sub-chapter 6.2), with access to the top of the welding seam. Since the temperatures reached during the FSW process are 70 – 90 % of the melting temperature of the merged materials (see § 1.3), and the material positioned at the top (AA7075) has a melting temperature of approximately 635 °C, a temperature evolution is expected during the process of 445 – 572 °C;
- the variations recorded were given by the fact that the highest temperature during the process is encountered at the interface between the active element and the joining materials, both in the pine and its shoulder area, areas that are not accessible to the thermographic temperature measuring chamber.

For the temperature analysis in the ABAQUS 6.13/ Explicit software, the TEMPMAVG module was used, which interprets the temperature of each discretization element as a weighted average of all the variable values in the respective element.

In the penetration phase of the active element in the joining materials, the simulated temperature was analyzed as an average of the temperatures of the discretization elements positioned behind the active element, in the upper area of the welding seam (to reproduce the area recorded by the thermographic chamber), at the end the penetration phase, respectively, in the second 4,9 simulation.

The total number of analyzed elements was 57, and the average of their temperatures was 523 °C. Compared to the temperature of 480 °C determined with the thermographic chamber at the end of the penetration stage, the difference is about 8 % and can be explained by the lack, in numerical simulation, of the step of maintaining the active element in the welding materials after the penetration phase.

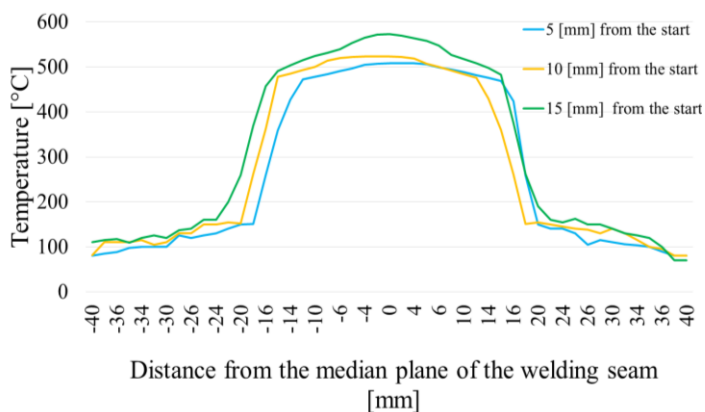


Fig. 9.2.4. Temperature variation in numerical simulation

Table 9.2.1. Average simulated temperatures in the shoulder area of the rotating active element

Position along the welding seam	The average of simulated temperatures [°C]
5 mm from the start	471
10 mm from the start	493
15 mm from the start	532

For the welding phase, the temperature evolution was determined in three different areas of the joint, perpendicular to the welding seam, at the top of it, positioned at 5 mm, 10 mm and 15 mm from the beginning of the welding seam, similar to the determination mode of the temperature during the welding process. The actual values of the simulated temperatures for all three different zones are shown in Fig. 9.2.4 and Table 9.2.1. As expected, in all three areas: the highest temperature is in the central part of the welding seam; the temperature increases with the approach of the rotating active element. The shape of the temperature curves is similar for all three positions analyzed.

It is noteworthy that, from the point of view of the temperature distributions obtained by simulation and, respectively, experimentally, no major differences are highlighted (Fig. 9.2.5 and Table 9.2.2). In both phases of the process - penetration and welding respectively - the average temperatures resulted by simulation are higher than the experimental average temperatures, but the differences do not exceed 8 % (Table 9.2.2).

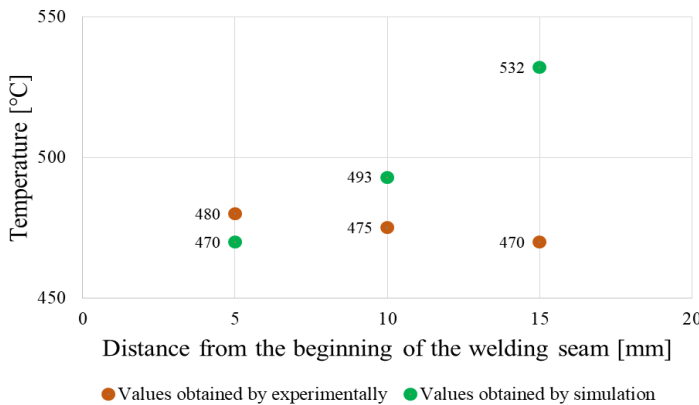


Table 9.2.2. Comparison between the average temperatures obtained by simulation and experimental

Phase	Average temperature [°C]	
	simulated	experimental
penetration	523	480
welding	499	475

Fig. 9.2.5. The evolution of the temperature obtained experimentally and, respectively, by simulation

The temperature values for the first 15 mm of the welding seam (Fig. 9.2.5 and Table 9.2.2) resulted from the numerical simulation (whose average was 499 °C) differs from those obtained experimentally (whose average was 475 °C) by 5,5 % – due to the method of experimental measurement of temperature and/ or hypotheses when defining the conditions of numerical simulation, so that it can be concluded that the numerical model is correct [B07].

Validation of the numerical model based on the aspect of the welding seam

This technique, although not one of the most common ones, can offer a direction regarding the veracity of the numerical model realized. The analysis concerned the penetration phase of the active element, the welding phase and, respectively, the defect distribution.

In the penetration phase of the active element, the appearance of the surface generated by simulation is similar to the aspect of the bore generated experimentally. In the welding phase, the distribution of the malleable material on the surface of the welding seam is similar in both cases (Fig. 9.2.6 and 9.2.7).

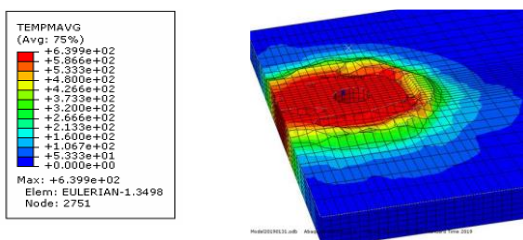


Fig. 9.2.6. The visual aspect of the welded seam simulated in the penetration phase of the active element

Fig. 9.2.7. The appearance of the welding seam made experimentally in the penetration phase and, respectively, in the withdrawal phase of the active element

Also, the area of appearance of the defects is represented by the advance part of the active element in the section of the welding seam, both in simulation and in the experimental study (Fig. 9.2.8 and 9.2.9).

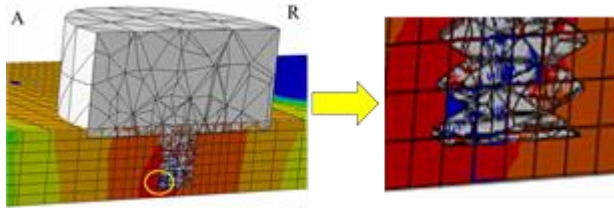


Fig. 9.2.8. The presence of defects in the section of the welding seam made by simulation

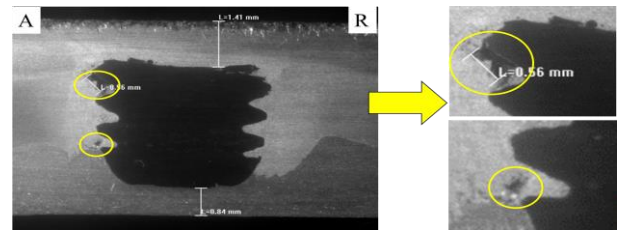


Fig. 9.2.9. The presence of defects in the section of the welding seam made experimentally

The deformations of the materials that appeared in the advance part of the numerical simulation are approximately similar to the deformations that appeared in the experimental study. Minor differences are given by the irregular shape of the welding seam along the joint (Fig. 9.2.10 and 9.2.11) [B07].

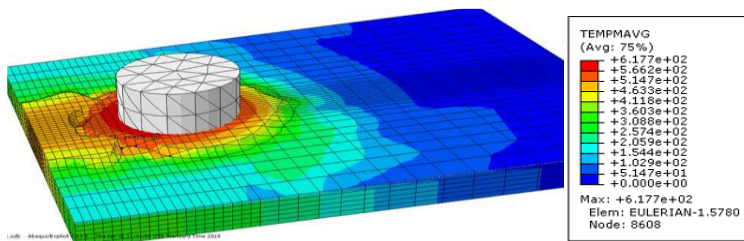


Fig. 9.2.10. The appearance of the welding seam made by numerical simulation



Fig. 9.2.11. The visual aspect of the welding seam made experimentally

By using two different validation techniques, which are based on comparing the temperatures and the weld seam appearance respectively, the numerical model made has been validated [B07];

The numerical model realized can be improved by using: some discretization elements with smaller dimensions in the welding seam area and on the depth of the welded structure, an Eulerian element that presents a more generous hollow area at the top of the welding seam, characteristics of the three aluminum alloys that vary according to temperature etc. which, of course, leads to an increase in the simulation duration [B07].

Chapter 10. Final conclusions and main contributions to the development and numerical modeling of the process and system of friction stir welding with rotating active element of different aluminum alloy structures

(1) From the analysis of the current state of research – development and industrial applications regarding the friction stir welding, important conclusions have been drawn, which are presented in chapter 4.

(2) In view of the data and conclusions from the analysis of the current state of research – development and industrial applications regarding the process and system of friction stir welding with active rotating element of the structures of aluminum alloys, the research – development directions were considered to be up to date as presented in § 5.1.

(3) In relation to the current stage and the directions of research – development regarding the friction stir welding of the structures of aluminum alloys, it was assumed as the main objective of the research – development activity in the doctorate (s. § 5.2): development of welding process and system with rotating active element of different aluminum alloy structures, through theoretical – experimental research and numerical modeling.

(4) The relevant conclusions regarding the doctoral research and development activity for achieving its main objective, noted from the preliminary theoretical – experimental researches performed according to the research – development methodology (s. § 5.3), are as follows.

○ The process temperature is directly influenced by the characteristics of the aluminum alloy positioned at the top of the welded structure, the highest temperatures being recorded for the structures where the AA7075 alloy is positioned at the top. The technological parameters have a varied influence on the temperature, respectively: the rotation speed directly influences the process temperature, and the increase of the welding speed determines a small increase of the temperature in the structure 3 – AA7075 positioned in the upper part, respectively, its decrease in the structures 1 and 2 – AA2024 alloy and, respectively, AA6061 positioned at the top, depending on the structure analyzed (s. § 7.2).

○ The axial process force is influenced by the technological parameters, respectively: the rotation speed influences inversely proportional, and the welding speed – directly proportional to the axial process force. The distance of stabilization of the axial force from the starting point of the welding seam is reduced as the period of retention of the active element increases at the end of the penetration phase, as well as the decrease of the welding speed (s. § 7.2).

○ The roughness value is directly influenced by the material positioned at the top of the working system. The lowest roughness values were recorded for structure 1 (AA2024 – positioned at the top), and the highest values of roughness were recorded for structure 3 (AA7075 – positioned at the top). Also, the variation of the values of the roughness depending on the technological parameters n and w differs from one structure to another, respectively: at structure 1 the increase of the two parameters leads to the decrease of the roughness, and for structures 2 and 3 the evolution of the roughness according to the technological parameters have a decreasing tendency with the welding speed rate increases (s. § 7.3).

○ The macrostructure of welded joints is influenced, to a large extent, by the structure analyzed, the fewest experiences that led to defects are associated with structure 3 (AA7075 – AA2024 – AA6061). The technological parameters have influenced the macrostructural characteristics at structure 1 - the best results are found in the area of the average values of the two technological parameters, and their increase negatively influences the macrostructural aspect, at structure 2 - the best results were recorded for the maximum rotation speed and the minimum value of the welding speed, and in structure 3 - the best results were recorded for the minimum value of the rotation speed and the variable welding speed (s. § 7.4).

○ At the macrostructural level, the creep between the three aluminum alloys is well highlighted, identifying the boundaries of delimitation between materials, which confirms the impossibility of mixing them at the molecular level. The best mixture of the three alloys and the smallest number of defects was corresponding to experience 3.1, respectively, in structure 3, with the minimum values of the technological parameters (s. § 7.5).

○ The values of microhardness are directly influenced by the macrostructure of the joint. The more the welded structure has a higher degree of mixing of the three materials, the greater the values of the microhardness. The variations recorded along the filaments of the three alloys in the welding seam, in comparison with the values of the microhardness of the basic materials, are, AA7075 shows a significant decrease of the values of the microhardness caused, to a large extent, by the thermal variation achieved during the process, AA2024 shows a decrease in the values of microhardness influenced, equally, both by the temperature reached during the process and by the degree of mixing of the three alloys along the welding seam, and AA6061 shows an increase in the values of microhardness due, to a large extent, mixing with the other two adjacent alloys (s. § 7.6).

(5) The relevant conclusions regarding the doctoral research and development activity for achieving its main objective, noted from the advanced theoretical – experimental research and the numerical simulations performed according to the research – development methodology (s. § 5.3), are as follows.

- The advanced theoretical – experimental researches were made on a single structure, respectively, structure 4 – in which the component plates are totally superimposed, and the materials – positioned as in structure 3 (s. § 8.1).
 - Increasing the rotation speed of the rotating active welding element increases the process temperature and decreases the axial process force, and increasing the welding speed leads to a small increase in the process temperature, but at the same time, an increase in the axial force process. The distance of stabilization of the process is influenced, to a large extent, by the retention period of the rotating active element at the end of the penetration phase, by the fact that a longer retention period produces a faster increase of the temperature (s. § 8.2).
 - The roughness of the welding seam is influenced by the technological parameters, respectively: it decreases with increasing the rotation speed and at the decrease of the welding speed. Also, the evolution of the roughness along the welding seam is stable, with decreasing tendency (s. § 8.3).
 - The macrostructural and microstructural analysis of the advanced experiments shows the following: increasing the rotation speed improves the shape and appearance of the welding zone of the welding seam, but at the same time it leads to the appearance of defects, and the increase of the welding speed decreases the rate of occurrence of defects in the section of the welding seam.
- Experience 4.3 (rotation speed 650 rpm and welding speed 100 mm/min) leads to the least number of defects. It was found that the best macrostructure of the joints is obtained for the technological parameters n and w of 600 – 650 rpm and, respectively, 70 – 100 mm/min (s. § 8.4 and 8.5).
- The distribution and the values of the microhardnesses in the welding seam are directly influenced by the macrostructure of the joint, the degree of mixing of the materials, the number of defects in the section of the welding seam and the stabilization of the process along the joint (samples x.x.2). The analysis of the values of the microhardnesses of the welded materials in comparison with the microhardnesses of the basic materials shows that in AA7075 and AA2024 there is a decrease compared to the basic materials, and in AA6061 – an increase compared to the basic material (s. § 8.6), similar to the variation recorded preliminary (s. § 7.6).
 - The mechanical properties – tensile strength of the welded pieces and relative elongation – for welded sample are directly influenced by the technological parameters of the process and the increase of the rotation speed leads to the decrease of the mechanical properties of the joint and the increase of the welding speed leads to the improvement of the mechanical properties, similar to the results of the macrostructural analysis. The highest value of the mechanical strength was recorded in the specimens with the best macrostructural aspect (exp. 4.3), achieved with the minimum value of rotation speed (650 rpm) and the maximum value of welding speed (100 mm/min). Compared to the mechanical strength of the basic materials, the value after welding is lower for AA7075 and AA2024 alloys, respectively, higher for AA6061 alloy. The relative elongation of all the analyzed specimens was smaller than that of the basic materials (s. § 8.7).
 - The numerical model made using the CEL method simulates experience 4.3, which led to the construction of a welded joint with the best features. This numerical model was validated by comparison with the results recorded in the experimental study, using the temperature distribution method and the welding seam appearance method. From the point of view of the temperatures obtained by simulation and, respectively, experimentally, the differences are of maximum 8 % – for the penetration phase of the rotating active element and of maximum 5,5 % – for the welding phase; from the point of view of the welding seam aspect, numerous similarities have been identified. It can be concluded that the numerical model made is valid (s. § 9.2).

(6) In achieving the main objective of the doctoral research – development activity, the present doctoral thesis brings a series of contributions, of which the most important ones are as follows.

- The elaborate study of the current state of research – development and industrial applications of friction welding with rotating active element.
- Application of the welding process by friction stir welding with an active rotating element under innovative conditions, respectively, for the realization of structures constituted by the superposition of three different aluminum alloy plates AA2024, AA6061, AA7075, alloys used on an industrial scale in the aeronautical industry and of which AA2024 it cannot be welded by standard procedures.
- Conducting theoretical – experimental researches preliminary and advanced complex and high volume, respectively, preparing the research system, carrying out four different types of welded structure under different welding technological conditions, measuring the temperature and axial process strength, sampling tests, analysis of some characteristics of the welding seam and the surrounding areas, graphical representation of specific dependency relationships, highlighting representative correlations and conclusions.
- Analysis, within the preliminary theoretical – experimental researches, at three different types of welded structure, process temperature, axial process force, as well as the roughness, macrostructure, microstructure and microstrength of the welding seam and the surrounding areas, with some correlations representations and conclusions.
- Analysis, within the theoretical – experimental researches advanced, to a certain type of welded structure, of the process temperature, the axial process force, as well as of the roughness, macrostructure, microstructure, microhardness tensile strength and relative elongation of the welding seam and the surrounding areas, with the highlighting of some representative correlations and conclusions.
- Development of a valid numerical model for simulating the FSW joint of three different aluminum alloys.

* * *

The present doctoral thesis, through the problematic, the approach and results mode, develops the conditions for deepening and applying the friction stir welding process of different aluminum alloy structures, through theoretical – experimental research and numerical modeling.

The scientific importance of this doctoral thesis is supported by the contributions made to the study, theoretical research – experimental and numerical modelling on the process and system of friction welding with rotating active element, FSW, of structures of three different aluminium alloys, AA2024, AA6061 and AA7075, in relation to methodological reference elements, by determining the dependency relationships between the process axial force and the process temperature according to the speed of the rotating active element, the speed of advance and attributes of the welding structure, between them and characteristics of the welded structures - roughness, macrostructure, microstructure, microhardness, tensile strength, relative elongation at breakage, as well as a valid numerical model for simulating the process and objective welding system.

The practical importance of this doctoral thesis lies in the fact that the research - development methodology, the models and means of working, the actual data and results of the research carried out are a system – useful support for students, teachers, specialists and industrial organisations, as appropriate.

The issue of FSW processes demands a research – development activity continuous of study and determination of optimal welding conditions and characteristics of welded joints for various materials, geometries, production volumes etc.

Selective references

- [A04] Al-Badour F., Nesar M., Abdelrahman S., Abdelaziz B., *Thermo-mechanical finite element model of friction stir welding of dissimilar alloys*, Int. Adv. Manuf. Technol. 72:607-617, 2014.
- [A08] Azevedo J., Infante V., Quintino L., Santos J., *Fatigue behaviour of friction stir welded steel joints*, 11th International Fatigue Congress Lisboa 2014.
- [B01] Babu A.S., Devanathan C., *An Overview of Friction Stir Welding*, International Journal of Research in Mechanical Engineering & Technology, 3, 2, 2013.
- [B02] Batalha G.F., Farias A., Magnabosco R., Delijaicov S., Adamiak M., Dobrzański L.A., *Evaluation of an AlCrN coated FSW tool*, J. of Achievements in Materials and Manufacturing Engineering, Volume 55, Issue 2, Decembrer 2012.
- [B03] Bhattacharya T. K., Das H., Pal T.K., *Influence of welding parameters on material flow, mechanical property and intermetallic characterization of friction stir welded AA6063 to HCP copper dissimilar butt joint without offset*, Trans. Nonferrous Met. Soc. China 25, pp. 2833–2846, 2015.
- [B05] Boromei I., Ceschini L., Morri A., G. Garagnani L., *Friction stir welding of aluminium based composites reinforced with Al₂O₃ particles: effects on microstructure and charpy impact energy*, Metallurgical Science and Technology, 24 (1), pp. 12-21, 2006.
- [B06] **Bosneag A.**, Constantin M.A., Nitu E., Ciuca C., *Analysis and Correlation of Output Parameters against Input Parameters for Friction Stir Welding of Three Dissimilar Aluminum Alloy*, Advanced Materials Research, Vol. 1146, pp. 38-43, ISSN: 1662-8985, doi:10.4028/www.scientific.net/AMR.1146.38, 2017 [Volum BDI] (presented: ISCS17 – Structural integrity of welded structures, The 12th International Conference, 09-10 November 2017, Timișoara, România).
- [B07] **Bosneag A.**, Constantin M. A., Nitu E., Iordache M., Badulescu C., *Numerical simulation of Friction Stir Welding of three dissimilar aluminium alloy*, Materials Science and Engineering, Vol. 564, Article Number 012033, doi:10.1088/1757-899X/564/1/012033, WOS: 000562599900033, 2019 [Volum ISI] (presented: IManEE19 – Innovative Manufacturing Engineering & Energy International Ceonference, The 23rd edition, 22-24 May, Pitești, România).
- [B08] **Bosneag A.**, Constantin M. A., Nitu E., *Study on Analysis between Friction Stir Welding Process and Hybrid Friction Stir Welding Process*, Annals of the "Constantin Brâncuși" University of Târgu-Jiu, Engineering Series, Issue 3, pp. 59-65, 2015 [Revistă BDI] (presented: CONFERENG 2015 – Conferință științifică națională cu participare internațională, 13-14 November, Universitatea "Constantin Brâncuși", Târgu-Jiu, România).
- [B09] **Bosneag A.**, Constantin M. A., Nitu E., Iordache M., Rizea A., *Friction Stir Welding of Composite Materials with Metallic Matrix: a Brief Review*, Applied Mechanics and Materials, Vol. 809-810, pp. 449-454, doi:10.4028/www.scientific.net/AMM.809-810.449, 2015 [Volum BDI] (presented: IManE2015 – Innovative Manufacturing Technology International Conference, The 19th edition, 20-22 May, Iași, România).
- [B10] **Bosneag A.**, Constantin M.A., Nitu E., Iordache M., *Analysis of the influence of position of welding materials on the FSW seams properties for three dissimilar aluminium alloy*, MATEC Web of Conferences, Vol. 178, Article Number 03003, doi: doi.org/10.1051/mateconf/201817803003, WOS: 000570197900032, 2018 [Volum ISI] (presented: IManE&E 2018 – Innovative Manufacturing Technology International Conference, The 22nd edition, 31 May – 2 June, Chișinău, Republica Moldova).
- [B11] **Bosneag A.**, Constantin M.A., Nitu E., Iordache M., *Friction Stir Welding of three dissimilar aluminium alloy: AA2024, AA6061 and AA7075*, IOP Conf. Series: Materials Science and Engineering, Vol. 400, 022013, doi: 10.1088/1757-899X/400/2/022013, WOS:000461147400013, 2018 [Volum ISI] (presented: ModTech 2018 – Modern Manufacturing Technologies in Industrial Engineering, The 6th International Conference, 13-16 June, Constanța, România).
- [B12] **Bosneag A.**, Constantin M.A., Nitu E., Iordache M., *Friction Stir Welding of three dissimilar aluminium alloy used in aeronautics industry*, IOP Conference Series - Materials Science and Engineering, Vol. 252, 012041, DOI: 10.1088/1757-899X/252/1/012041, WOS:000419817200041, ISSN: 1757-8981, 2017 [Volum ISI] (presented: CAR 2017 – The International Congress of Automotive and Transport Engineering, 8-10 November, Pitești, România).

- [B16] Burek R., Wydrzynski D., Sep J., Wieckowski W., *The effect of tool wear on the quality of lap joints between 7075 T6 aluminum alloy sheet metal created with the FSW method*, Maintenance and Reliability, 20, 1, pp. 100-106, 2018.
- [C01] Campanelli S. L., Casalino G., Casavola C., Moramarco V., *Analysis and Comparison of Friction Stir Welding and Laser, Assisted Friction Stir Welding of Aluminum Alloy*, Materials 2013, Vol. 6, pp. 5923-5941, 2013.
- [C03] Casavola C., Cazzato A., Moramarco V., *Residual Stress in Friction Stir Welding and Laser – Assisted Friction Stir Welding by Numerical Simulation and Experiments*, IntechOpen, 2018.
- [C09] Commin L., Barrallier L., Masse J. E., *Residual stress evolution analysis in AZ31 friction stir welds using X-RAY and neutron diffraction*, Int. Centre for Diffraction Data, 2009.
- [C10] Constantin M. A., **Bosneag A.**, Iordache M., Nitu E., Iacomi D., *Numerical Simulation of Friction Stir Welding of Aluminum Alloys: A Brief Review*, Applied Mechanics and Materials, Vol. 809-810, pp. 467-472, doi:10.4028/www.scientific.net/AMM.809-810.467, 2015 [Volum BDI] (presented: IManE2015 – Innovative Manufacturing Technology International Conference, The 19th edition, 20-22 May, Iași, România).
- [C12] Constantin M. A., **Bosneag A.**, Nitu E., Botila L., *Establishing the Dependence of Output Parameters Depending on Local Process Conditions for Friction Stir Welding of Pure Copper Plates*, Advanced Materials Research, ISSN 1662-8985, Vol. 1146, pp. 32-37, doi: 10.4028/www.scientific.net/AMR.1146.32, 2017 [Volum BDI] (presented: ISCS17 – Structural integrity of welded structures, The 12th International Conference, 09-10 November, Timișoara, România).
- [C13] Constantin M. A., **Bosneag A.**, Nitu E., Iordache M., *Comparative study on microhardness between friction stir welding and tungsten inert gas assisted friction stir welding of pure copper*, MATEC Web of Conferences, Vol. 178, Article number 03002, doi: doi.org/10.1051/mateconf/201817803002, WOS: 000570197900031, 2018 [Volum ISI] (presented: IManE&E 2018 – Innovative Manufacturing Technology International Conference, The 22nd edition, 31 May – 2 June, Chișinău, Republica Moldova).
- [C14] Constantin M. A., **Bosneag A.**, Nitu E., Iordache M., *Experimental investigations of tungsten inert gas assisted friction stir welding of pure copper plates*, IOP Conference Series - Materials Science and Engineering, Vol. 252, 012038, DOI: 10.1088/1757-899X/252/1/012038, WOS: 000419817200038, ISSN: 1757-8981, 2017 [Volum ISI] (presented: CAR 2017 – The International Congress of Automotive and Transport Engineering, 8-10 November, Pitești, România).
- [C15] Constantin M. A., **Bosneag A.**, Nitu E., Iordache M., *Orientation of process parameter values of TIG assisted FSW of copper to obtain improved mechanical properties*, IOP Conf. Series: Materials Science and Engineering, Vol. 400, 022017, doi: 10.1088/1757-899X/400/2/022017, WOS:000461147400017, 2018 [Volum ISI] (presented: ModTech 2018 – Modern Manufacturing Technologies in Industrial Engineering, The 6th International Conference, 13-16 June, Constanța, România).
- [C16] Constantin M. A., Nitu E., Badulescu C., *Numerical simulation of friction stir welding of pure copper plates*, Materials Science and Engineering, Vol. 564, 012031, 2019.
- [C17] Craçanel M., **Bosneag A.**, Diakhate M., Badulescu C., Nitu E., Iordache M., Grigore J., *Influence des paramètres du procédé de soudage FSW sur le comportement mécanique de l'assemblage : analyse par émission acoustique et corrélation d'images numériques*, 24^{ème} Congrès Français de Mécanique Brest, pp. 6360-6368, sciencesconf.org:cfm2019:244191, 2019 [Volum BDI] (presented: CFM19 24^{ème} Congrès Français de Mécanique, 26 - 30 August, Brest, France).
- [C18] Czigany T., Kiss Z., *Friction stir welding of fiber reinforced polymer composites*, 18th International Conference On Composite Materials, 2011.
- [D07] Diogo M.N., Pedro N., *Numerical modeling of friction stir welding process: a literature review*, The Int. J. of Advanced Manufacturing Tech., Vol. 65, pp. 115-126, 2013.
- [D10] Dong J., Zhang D., Zhang W., Zhang W., Qiu C., *Microstructure Evolution during Dissimilar Friction Stir Welding of AA7003-T4 and AA6060-T4*, Materials, 11, 342, 2018.
- [E01] Elnabi M. M. A., Osman T. A., Mokadem A. E. E., Elshalakany A. B., *Modeling and Optimization of Friction Stir Welding Parameters for Joining Dissimilar Aluminum Alloys*, Advance Journal of Graduate Research, Vol. 4, No. 1, pp. 1-14, 2018.

- [E02] El-Sayed M.M., Shash A.Y., Abd-Rabou M., *Finite element modeling of aluminum alloy AA5083-O friction stir welding process*, Journal of Materials Processing Technology, Vol. 252, pp. 13-24, 2018.
- [F01] Fanelli P., Vivio F., Vullo V., *Experimental and numerical characterization of Friction Stir Spot Welded joints*, Engineering Fracture Mechanics, Vol. 81 pp. 17–25, 2012.
- [G06] Grigore J-C., **Bosneag A.**, Badulescu C., *Tensile properties of friction stir welding of three dissimilar aluminium alloys, AA7075, AA2024 and AA6061 versus process parameters*, Materials Science and Engineering, Vol. 564, Articol Number 012034, doi:10.1088/1757-899X/564/1/012034, 2019 [Volum ISI] (presented: IManEE19 – Innovative Manufacturing Engineering & Energy International Conference, The 23rd edition, 22-24 May, Pitești, România).
- [J01] Jain R., Pal S.K., Singh S.B., *Finite Element Simulation of Temperature and Strain Distribution during Friction Stir Welding of AA2024 Aluminum Alloy*, J. Inst. Eng. India, Ser. C, Vol. 98, pp. 37–43, 2017.
- [J02] Jemal N., *Qualification du domaine de soudabilité en soudage par friction malaxage*, Doctorat ParisTec -THÈSE pour obtenir le grade de docteur délivré par l'École Nationale Supérieure d'Arts et Métiers Spécialité "Génie Mécanique", le 13 décembre 2011.
- [J03] Johnson G.R., Cook W.H., *Fracture Characteristics of Three Metals Subjected to Various Strains, Strain Rates, Temperatures and Pressures*, Engineering Fracture Mechanics., Vol. 21, pp. 31-48, 1985.
- [K02] Kalemba-Rec I., Kopyscianski M., Miara D., Krasnowski K., *Effect of process parameters on mechanical properties of friction stir welded dissimilar 7075-T651 and 5083-H111 aluminum alloys*, Int. J. Adv. Manuf. Technol., Vol. 97, pp. 2767–2779, 2018.
- [K05] Khalilabad M.M., Zedan Y., Texier D., Jahazi M., Bocher P., *Effect of tool geometry and welding speed on mechanical properties of dissimilar AA2198-AA2024 FSWed joint*, Journal of Manufacturing Processes, Vol. 34, pp. 86-95, 2018.
- [K06] Khan N. Z., Siddiquee A. N., Khan Z. A., Shihab S. K., *Investigations on tunneling and kissing bond defects in FSW joints for dissimilar aluminum alloys*, J. of Alloys and Compounds, Vol. 648, pp. 360-367, 2015.
- [K09] Kirk F., Lyne S., Laszlo I. K., *A Mesh-Free Solid-Mechannics Approach for Simulating the Friction Stir-Welding Process*, INTECH, 2016.
- [K10] Kiss Z., Czigany T., *Applicability of friction stir welding in polymeric materials*, Mechanical Engineering, 51(1), 15–18, 2007.
- [K12] Krasnowski K., Hamilton C., Dymek S., *Influence of the tool shape and weld configuration on microstructure and mechanical properties of the Al 6082 alloy FSW joints*, Archives of civil and mechanical engineering 15, pp. 133 – 141, 2015.
- [L02] Leitao C. M. A., *Influence of base material plastic properties and process parameters on friction stir weldability*, Universidad de Coimbra, 2013.
- [L06] Lorrain O., *Analyses expérimentale et numérique du procédé de soudage par friction malaxage FSW*, These, Doctorat ParisTech, 2010.
- [M01] Magalhaes V.M., Leitao C., Rodrigues D.M., *Friction stir welding industrialisation and research status*, Science and Technology of Welding and Joining, 2017.
- [M04] Meilinger A., Török I., *The importance of Friction Stir Welding Tool*, Production Processes and Systems, vol. 6., No. 1, pp. 25-34, 2013.
- [M05] Meyghani B., Awang M.B., Emamian S.S., Nor M.K.M., Pedapati S.R., *A Comparison of Different Finite Element Methods in the Thermal Analysis of Friction Stir Welding (FSW)*, MDPI, 7, 450, 2017.
- [M06] Minak G., Ceschini L., Boromei I., Ponte M., *Fatigue properties of friction stir welded particulate reinforced aluminium matrix composites*, Int. J. of Fatigue, Vol. 32, pp. 218–226, 2010.
- [M07] Mishra A., *Friction Stir Welding Of Dissimilar Metal: A Review*, IJRASET, 6, pp. 2321-9653, 2018.
- [M09] Mishra R.S., Ma Z.Y., *Friction stir welding and processing*, Materials Science and Engineering, Vol. 50, pp. 1–78, 2005.
- [M12] Montadhar A., *A Mathematical and Experimental Analysis of Friction Stir Welding of Steel*, Collaborating Organization TWI Yorkshire, 2018.

- [M15] Mroczka K., Pietras A., *FSW characterization of 6082 aluminium alloys sheets*, Int. Scientific J. published monthly by the World Academy of Materials and Manufacturing Engineering, 40 (2), pp. 104-109, 2009.
- [N01] Nakata K., Kim Y.G., Ushio M., Hashimoto T., Jyogan S., *Weldability of high strength aluminium alloys by friction stir welding*, ISIJ Int. 40, pp. 515-519, 2000.
- [N03] Neto D.M., Neto P., *Numerical modeling of friction stir welding process: a literature review*, Int J Adv Manuf Technol, 65:115–126, 2013.
- [P05] Pankul G., Arshad N.S., Noor Z.K., Mohd A.H., Zahid A.K., Mustufa H.A., Abdulrahman A., *Investigation of the Effect of Tool Pin Profile on Mechanical and Microstructural Properties of Friction Stir Butt and Scarf Welded Aluminium Alloy 6063*, MDPI Journal Metals, 8, 74, 2018.
- [P07] Pashazadeh H., Masoumi A., Teimournezhad J., *Numerical modelling for the hardness evaluation of friction stir welded copper metals*, Materials and Design 49, pp. 913–921, 2013.
- [P10] Prakash D., Gurunath S., *Perspective of Friction Stir Welding Tools*, Materials Today: Proceeding, 5, pp. 13166-13176, 2018.
- [R01] Rahul J., Surjya K.P., Shiv B.S., *Numerical modeling methodologies for friction stir welding process*, Computational Methods and Production Engineering, Indian Institute of Technology, Kharagpur, India, 2017.
- [R03] Robe H., Zedan Y., Chen J., Monajati H., Feulvarch E., Bocher P., *Microstructural and mechanical characterization of a dissimilar friction stir welded butt joint made of AA2024-T3 and AA2198-T3*, Materials Characterization, Vol. 110, pp. 242-251, 2015.
- [R08] Radeș M., *Rezistența materialelor 1*, Editura Printech, 2010.
- [S01] Sadeesh P., Venkatesh K. M., Rajkumar V., Avinash P., Arivazhagan N., Devendranath R. K., Narayanan S., *Studies on friction stir welding of AA2024 and AA6061 dissimilar metals*, Procedia Engineering, Vol. 75, pp. 145-149, 2014.
- [S03] Sanjeev N.K., Ravikiran B.P., *Application of Coupled Eulerian Lagrangian Approach in Finite Element Simulation of Friction Stir Welding*, 2015.
- [S12] Song K. H., Tsumura T., Nakata K., *Development of Microstructure and Mechanical Properties in Laser-FSW Hybrid Welded Inconel 600*, Materials Transactions. 50(7), pp. 1832-1837, 2009.
- [S17] Syafiq W.M., Afendi M., Daud R., Mazlee M.N., Majid M.S.A., Lee Y.S., *Mechanical properties of friction stir welded butt joint of steel/ aluminium alloys: effect of tool geometry*, Journal of Physics, 908, 2017.
- [S18] ***, SR EN ISO 6892-1, *Materiale metalice, Încercarea la tracțiune, Partea 1: Metoda de încercare la temperatura ambiantă*, STANDARD ROMÂN, 2010.
- [S19] ***, ASTM E112-96 (2004), *Standard Test Methods for Determining Average Grain Size*, ASTM International, 2004.
- [S20] Szava I., Szava D.T., Galfi P.B., Hoța H., Szava I.R., Popa G., *Rezultate preliminare privind utilizarea metodei corelării digitale a imaginii în studiul implanturilor dentare*, A XVII-a Conferință internațională – multidisciplinară “Profesorul Dorin Pavel – fondatorul hidroenergeticii românești”, SEBEȘ, 2017.
- [T02] ***, The Boeing Company, http://www.boeing.com/commercial/aeromagazine/articles/qtr_4_06/article_04_2.html (accesat la 09.06.2017).
- [T06] Thomas W.M., Nicholas E.D., Needham J.C., Murch M.G., Temple-Smith P., Dawes C.J., *International Patent Application No. PCT/GB92/02203 and GB Patent Application No. 9125978.8 and US Patent Application No. 5,460,317*, December 1991.
- [U01] Ungureanu I., *Bazele cercetării experimentale*, Editura Universității din Pitești, 2001.
- [V03] ***, Vickers hardness tester, <https://www.innovatest-europe.com/testing-knowledge/> (accessed on 20.07.2020).